The one-dimensional Kondo lattice model studied by the density matrix renormalization group method

1999 J. Phys.: Condens. Matter 11 R1

(http://iopscience.iop.org/0953-8984/11/2/002)

J. Phys.: Condens. Matter **11** (1999) R1–R30. Printed in the UK PII: S0953-8984(99)97037-6

REVIEW ARTICLE

The one-dimensional Kondo lattice model studied by the density matrix renormalization group method

Naokazu Shibata† and Kazuo Ueda‡

† Institute of Applied Physics, University of Tsukuba, Tsukuba 305-8573, Japan
‡ Institute for Solid State Physics, University of Tokyo, 7-22-1 Roppongi, Minato-ku, Tokyo 106-8666, Japan

Received 26 August 1998

Abstract. Recent developments in the theoretical investigation of the one-dimensional Kondo lattice model by using the density matrix renormalization group (DMRG) method are discussed in this review. Short summaries are given of the zero-temperature DMRG method, the finite-temperature DMRG method, and also the application of the finite-T DMRG to dynamic quantities.

Away from half-filling, the paramagnetic metallic state is shown to be a Tomonaga–Luttinger liquid with a large Fermi surface. The size of the large Fermi surface is determined by the sum of the densities of the conduction electrons and the localized spins. The correlation exponent K_ρ of this metallic phase is smaller than 1/2. At half-filling the ground state is insulating. The excitation gaps are different, depending on the channels, the spin gap, the charge gap and the quasiparticle gap. The temperature dependence of the spin and charge susceptibilities and the specific heat are discussed. Particularly interesting is the temperature dependence of various excitation spectra, which indicates unusual properties for the Kondo insulators.

1. Introduction

For a degenerate Fermi gas, the low-temperature specific heat is linear in T and the proportionality constant is given by the density of states at the Fermi energy. For the free electrons the density of states including the two spin directions is given by

$$D(\epsilon_{\mathrm{F}}) = \frac{mk_{\mathrm{F}}}{\pi^2\hbar^2} \tag{1}$$

where m is the free-electron mass and k_{F} is the Fermi wavenumber.

To include the effect of the electron–electron interaction, Landau developed the theory of Fermi liquids. Since the volume of the Fermi sphere is determined by the density of electrons, it is a reasonable assumption that the Fermi wavenumber is not changed by the interaction; this was in fact proven later by Luttinger [1]. According to Landau, the effect of the interaction can be taken into account by replacing the bare-electron mass m by an effective mass m^*. Thus the importance of interaction effects in each material may be judged from the electronic specific heat at low temperatures.

For ordinary metals the coefficient of the T-linear term, γ, is of the order of mJ mol^{-1} K^{-2}. However, among the rare-earth and actinide compounds there is a group of compounds whose γ-values are in the range from 0.1 J mol^{-1} K^{-2} to more than 1 J mol^{-1} K^{-2}. This class of materials is called the heavy-fermion system or heavy-electron system. A key feature of the heavy-fermion system is that it contains two different types of electron: relatively localized

0953-8984/99/020001+30$19.50

f electrons and extended conduction electrons. The interplay between the two degrees of freedom is the essence of the heavy-fermion physics.

Since the Coulomb interaction between the f electrons is strong, a partially filled f shell in an isolated ion possesses a well defined magnetic moment corresponding to the total angular momentum of the f shell. A weak hybridization between the f electrons and the conduction electrons is a source of interesting many-body problems.

When we consider a single f shell in the sea of conduction electrons, the magnetic moment of the f electrons is unstable, leading to the Kondo singlet which is a bound state of the f moment with the spin polarization of the conduction electrons [2]. When we consider two f shells, the spin polarization of the conduction electrons induced by an f moment tends to stabilize the magnetic moment of the other f shell. This is the origin of the Ruderman–Kittel–Kasuya–Yosida (RKKY) interaction [3]. Thus the Kondo effect and the RKKY interaction in many cases compete with each other.

If the Kondo effect dominates over the RKKY interaction for some reason, a paramagnetic heavy-fermion state will be stabilized. In this regime, the Kondo temperature or the effective Fermi temperature in a lattice problem sets a small energy scale at low temperatures. The existence of the small energy scale naturally leads to a large specific heat, since the entropy associated with the magnetic degrees of freedom of f orbitals should be released in the small temperature range.

The simplest theoretical model for the heavy-fermion physics is the Kondo lattice model. The Kondo lattice model is given by

$$\mathcal{H} = \sum_{\langle ij \rangle} \sum_{s} t_{ij} c_{is}^{\dagger} c_{js} + J \sum_{i} \sum_{s,s'} \boldsymbol{S}_i \cdot \frac{1}{2} \boldsymbol{\sigma}_{ss'} c_{is}^{\dagger} c_{is'} \tag{2}$$

where the $\boldsymbol{\sigma} = (\sigma_x, \sigma_y, \sigma_z)$ are the Pauli matrices and $\boldsymbol{S}_i = \sum_{s,s'} \frac{1}{2} \boldsymbol{\sigma}_{ss'} f_{is}^{\dagger} f_{is'}$ is the f-electron spin at site i. In this review we will consider the model with only nearest-neighbour hoppings, $t_{ij} = -t$, for the nearest-neighbour pairs.

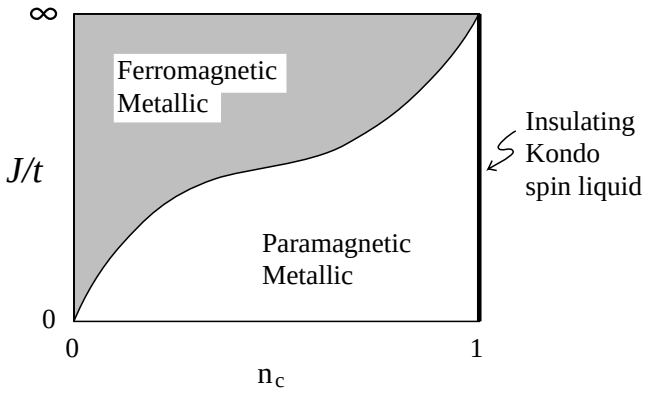

Figure 1. The ground-state phase diagram for the one-dimensional Kondo lattice model with nearest-neighbour hoppings.

Much effort has been invested in the study of the model and significant progress has been achieved for one dimension in the last ten years [4]. When we fix a lattice structure, the Kondo lattice model has only two parameters: one is the density of conduction electrons n_c and the other is the strength of the exchange coupling normalized with respect to the hopping energy J/t. In one dimension, the ground-state phase diagram in the parameter space is completed and this is shown in figure 1.

There are three different phases in the phase diagram. In the region from the low-density limit to the strong-coupling limit, a ferromagnetic metallic phase is stabilized. The spin quantum number in this phase is given by $S_{\rm tot} = (L - N_{\rm c})/2$, where L is the number of lattice sites and $N_{\rm c}$ is the number of conduction electrons. Note that the magnetic moment vanishes as half-filling is approached. The line of half-filling is special in the sense that the ground state is always a non-magnetic insulator. Since the lowest excitation in this phase is a spin-triplet excitation with a finite excitation gap, this phase is called an incompressible spin-liquid phase. In the remaining part of the phase diagram (figure 1) which extends from the weak-coupling limit towards the line of half-filling, the ground state is metallic and paramagnetic. In this review we will discuss properties of the spin-liquid phase and the paramagnetic metallic phase.

The existence of the small energy scale in the Kondo lattice model means that correlation lengths are generally long. For example, to study the spin gap and the charge gap in the spin-liquid phase, exact diagonalization was used at first [5]. However, the largest system size which can be diagonalized by the Lanczos algorithm is just ten sites. This is why a non-trivial form of a finite-size scaling was necessary for obtaining the functional form of the spin gap.

Recently, Steven White developed the density matrix renormalization group (DMRG) method to study the ground-state properties of one-dimensional many-body systems [6]. The advantage of this method is that systems that are an order of magnitude bigger can be studied, as compared with the case for numerical exact diagonalization by the Lanczos algorithm. Unlike quantum Monte Carlo simulations, the DMRG method is free from statistical errors. The numerical errors in the DMRG method are truncation errors, but they can be estimated from the largest eigenvalue of the density matrix which is truncated out. The truncation error may be lessened by increasing the number of basis states for the density matrix. The DMRG method is an ideal tool for studying the one-dimensional Kondo lattice model and in this review we will discuss recent developments on this subject.

Further development of the DMRG method was achieved last year when Wang and Xiang [7] and one of the authors [8] independently succeeded in obtaining thermodynamic properties of the one-dimensional quantum XXZ-model by applying the DMRG method to the transfer matrix (the finite-T DMRG method). Application of the finite-T DMRG method to a system with fermion degrees of freedom started from the Kondo lattice model [9].

The present article is organized as follows. In the next section, after a brief summary of the DMRG method for the ground state, we will describe the method used to calculate thermodynamic properties by the finite-T DMRG method and then extend discussions to the dynamic quantities at finite temperatures. In section 3 the nature of the paramagnetic metallic phase away from half-filling is shown to be that of a Tomonaga–Luttinger liquid with a large Fermi surface. The large Fermi surface means that the volume inside the Fermi surface is determined not only by the density of conduction electrons but also includes the localized spins. Section 4 is devoted to the discussion of the spin-liquid phase at half-filling. After the discussion of the spin gap and the charge gap at zero temperature, we will discuss how the excitation gaps develop as the temperature is lowered. We will conclude the present review by giving a summary and discussion in section 5.

2. The density matrix renormalization group method

The density matrix renormalization group (DMRG) method is relatively new [6] among the various numerical algorithms used to treat many-body problems. However, it is now widely used as one of the most standard numerical methods for treating low-dimensional many-body systems.

In this section we first briefly outline the algorithm of the zero-temperature DMRG method that was developed to study the ground-state and the low-energy excitations of one-dimensional systems. The application of this method to the quantum transfer matrix enables us to obtain thermodynamic quantities [8, 7] and the dynamical correlation functions at finite temperatures. In the second part of this section we will summarize the algorithm of the finite-T DMRG method.

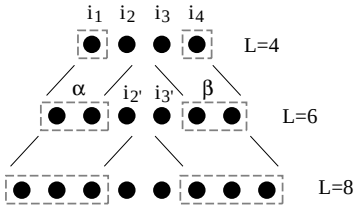

Figure 2. A schematic diagram of the infinite-system algorithm of the DMRG method.

2.1. The zero-temperature algorithm

The zero-temperature DMRG method is designed to obtain the ground-state wave function and the low-energy excitations with small systematic errors. The ground-state wave function and the low-energy excitations of long systems are obtained by expanding the system size iteratively as shown in figure 2. The expansion of the system is achieved by putting additional sites in its central region to minimize the undesirable boundary effects on the added sites. The algorithm is described in the following.

Let us start from a system of four identical sites—for example, a four-site spin chain under open boundary conditions. An operator on the nth site, e.g. S_n, is represented in terms of the complete basis states $|i_n\rangle$ as

$$\langle i_n|S_n|i_n'\rangle = (S_n)_{i_n,i_n'}. \tag{3}$$

Then we construct a representation of the Hamiltonian $H_{i_1i_2i_3i_4,i_1'i_2'i_3'i_4'}$ for the total system. The ground-state eigenvector

$$|\Psi_{i_1i_2i_3i_4}\rangle = \Psi_{i_1i_2i_3i_4}|i_1\rangle|i_2\rangle|i_3\rangle|i_4\rangle \tag{4}$$

is obtained by diagonalizing the Hamiltonian matrix by some method like the Lanczos algorithm. Then $\Psi_{i_1i_2i_3i_4}$ is used to construct the density matrix

$$\rho_{i_1i_2,i_1'i_2'} = \sum_{i_3i_4} \Psi_{i_1i_2i_3i_4}\Psi^*_{i_1'i_2'i_3i_4} \tag{5}$$

for the block containing the sites $n = 1$ and 2. The density matrix specifies to what extent the basis states $|i_1\rangle|i_2\rangle$ of the block are contributing to the total wave function $|\Psi_{i_1i_2i_3i_4}\rangle$. This matrix is numerically diagonalized, and we obtain its eigenvalues λ^α and eigenvectors $v^\alpha_{i_1i_2}$. Then we select the eigenvectors of the largest m eigenvalues as the new basis states for the block. Here m is the number of the basis states retained for the block at the next step. Using the selected eigenvectors of the density matrix we represent the operators on the site, for example, $n = 2$, as

$$(S_2)_{\alpha,\alpha'} = \sum_{i_1i_2i_2'} (S_2)_{i_2,i_2'}(v^\alpha_{i_1i_2})^* v^{\alpha'}_{i_1i_2'}. \tag{6}$$

A similar procedure is repeated for the block containing the sites $n = 3$ and 4, and all operators in the original system are represented in terms of the new basis states:

$$|\alpha\rangle = \sum_{i_1 i_2} v^{\alpha}_{i_1 i_2} |i_1\rangle |i_2\rangle \tag{7}$$

$$|\beta\rangle = \sum_{i_3 i_4} v^{\beta}_{i_3 i_4} |i_3\rangle |i_4\rangle. \tag{8}$$

To increase the size of the system we introduce two new sites between the blocks $n = 1, 2$ and $n = 3, 4$. Using the basis states $|i_{2'}\rangle$ and $|i_{3'}\rangle$, for the new sites, we construct the Hamiltonian matrix of the expanded system: $H_{\alpha i_{2'} i_{3'} \beta, \alpha' i'_{2'} i'_{3'} \beta'}$. Renaming the indices as follows:

$$\alpha \to i_1 \qquad i_{2'} \to i_2 \qquad i_{3'} \to i_3 \qquad \beta \to i_4 \tag{9}$$

we repeat the procedures from the diagonalization of the Hamiltonian matrix.

The key feature of the above renormalization procedure is that the new basis states $|\alpha\rangle$ or $|\beta\rangle$ of each block contain the information that the block is a part of the total system. As shown in figure 2, the edge part of each block connecting to the remaining part of the system is located in the middle of the system, and this part is not so sensitive to the boundary conditions imposed on the total system. Thus we expect the new basis states to also dominantly contribute to the ground-state wave function of the expanded system which has the two additional sites in the middle of the two blocks.

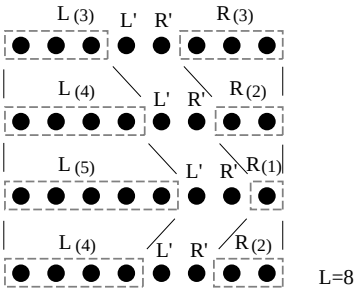

Figure 3. A schematic diagram of the finite-system algorithm of the DMRG method.

The above algorithm is called the infinite-system algorithm of the DMRG method. Using this algorithm we increase the size of the system. In order to improve the basis states of the blocks, it is necessary to fix the size of the system and use the following algorithm which is known as the finite-system algorithm of the DMRG method. A schematic diagram of the finite-system algorithm is shown in figure 3.

Let us take the block of size $n - 1$ on the left and the other block of size $n - 1$, whose basis states are represented by $|v^i_{L(n-1)}\rangle$ and $|v^i_{R(n-1)}\rangle$, on the right. These basis states and the representations of the operators in the blocks are obtained after the $(n - 2)$th renormalization step from the initial four-site system. The system of size $2n$ is constructed by inserting two additional sites for which the basis states are represented by $|i_{L'}\rangle$ and $|i_{R'}\rangle$.

We again diagonalize the Hamiltonian matrix of this $2n$-site system, namely $H_{i_{L(n-1)} i_{L'} i_{R'} i_{R(n-1)}, i'_{L(n-1)} i'_{L'} i'_{R'} i'_{R(n-1)}}$, and obtain the ground-state wave function $\Psi_{i_{L(n-1)} i_{L'} i_{R'} i_{R(n-1)}}$. Then we construct the density matrix

$$\rho_{i_{L(n-1)} i_{L'}, i'_{L(n-1)} i'_{L'}} = \sum_{i_{R'} i_{R(n-1)}} \Psi_{i_{L(n-1)} i_{L'} i_{R'} i_{R(n-1)}} \Psi^*_{i'_{L(n-1)} i'_{L'} i_{R'} i_{R(n-1)}} \tag{10}$$

for the subspace spanned by $|v^i_{L(n-1)}\rangle$ and $|i_{L'}\rangle$. We use the m important eigenvectors of this density matrix as the new basis states of the block containing n sites, and represent all operators in the new block in terms of the new basis states.

In the next step, we take the new left-hand block with n sites and the right-hand block with $n-2$ sites. The right-hand block with $n-2$ sites has been obtained at the $(n-3)$th renormalization step from the initial four-site system. Inserting two sites between these blocks, we construct the Hamiltonian matrix of the total system, $H_{i_{L(n)}i_{L'}i_{R'}i_{R(n-2)},i'_{L(n)}i'_{L'}i'_{R'}i'_{R(n-2)}}$, and repeat all of the above procedures.

We continue to increase (decrease) the size of the left-hand (right-hand) block until the right-hand block is reduced to a single site. Then we turn to decreasing (increasing) the size of the left-hand (right-hand) block in order to improve the basis states of the right-hand block. We continue to decrease (increase) the size of the left-hand (right-hand) block until the left-hand block is reduced to a single site. These procedures are continued back and forth until we get a good convergence.

In general, the total energy of the system is lowered as the basis states of the blocks are reconstructed. Thus, the lowest energy is obtained after the convergence. The wave function obtained by the finite-system algorithm of the DMRG method may be represented in a matrix product form [10]. Therefore the finite-system algorithm of the DMRG method is considered to be a numerical variational method which uses the matrix product wave function. This is another reason for our being able to achieve remarkable accuracy by the DMRG method. The accuracy of the ground-state energy and the wave function is determined by the eigenvalues of the density matrix which are truncated out. Thus we can improve the accuracy by increasing the number of basis states m used in the calculations so long as the memory of the computer allows.

2.2. The finite-temperature algorithm

It is also possible to discuss thermodynamic quantities using a DMRG method: the finite-T DMRG method. The readers who are not interested in the detail of the iteration procedures may skip the paragraphs including equations (13) to (26). In this method we use the quantum transfer matrix defined as

$$\begin{aligned}\mathcal{T}_{n(M)} &= [\mathrm{e}^{-\beta h_{2n-1,2n}/M}\mathrm{e}^{-\beta h_{2n,2n+1}/M}]^M \\ &= \sum_{\sigma_{2n\tau_1}}\sum_{\sigma_{2n\tau_{\underline{1}}}}\sum_{\sigma_{2n\tau_2}}\cdots\sum_{\sigma_{2n\tau_M}}\sum_{\sigma_{2n\tau_{\underline{M}}}}\langle\sigma_{2n-1,\tau_1}\sigma_{2n-1,\tau_{\underline{1}}}|\mathrm{e}^{-\beta h_{2n-1,2n}/M}|\sigma_{2n,\tau_1}\sigma_{2n,\tau_{\underline{1}}}\rangle \\ &\quad\times\langle\sigma_{2n,\tau_{\underline{1}}}\sigma_{2n,\tau_2}|\mathrm{e}^{-\beta h_{2n,2n+1}/M}|\sigma_{2n+1,\tau_{\underline{1}}}\sigma_{2n+1,\tau_2}\rangle \\ &\quad\times\langle\sigma_{2n-1,\tau_2}\sigma_{2n-1,\tau_{\underline{2}}}|\mathrm{e}^{-\beta h_{2n-1,2n}/M}|\sigma_{2n,\tau_2}\sigma_{2n,\tau_{\underline{2}}}\rangle \\ &\quad\vdots \\ &\quad\times\langle\sigma_{2n,\tau_{\underline{M}}}\sigma_{2n,\tau_1}|\mathrm{e}^{-\beta h_{2n,2n+1}/M}|\sigma_{2n+1,\tau_{\underline{M}}}\sigma_{2n+1,\tau_1}\rangle. \qquad (11)\end{aligned}$$

This quantum transfer matrix is shown graphically in figure 4. Here M is the Trotter number and τ_i is the discretized imaginary time whose intervals $\tau_{i+1}-\tau_i=\beta_0=\beta/M$. In equation (11), σ_{2n,τ_i} represents states of the site $2n$ corresponding to a given imaginary time τ_i. The Hamiltonian H is assumed to be decomposed into two parts $H_{\mathrm{odd}}=\sum_{n=1}^{L/2}h_{2n-1,2n}$ and $H_{\mathrm{even}}=\sum_{n=1}^{L/2}h_{2n,2n+1}$ so that we can evaluate the matrix element of the exponential function. Since the partition function Z is given by the trace of the product of the quantum transfer

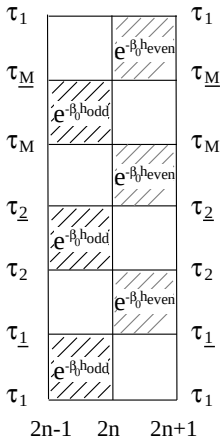

Figure 4. The quantum transfer matrix for $M = 3$. $h_{\rm odd}$ and $h_{\rm even}$ represent $h_{2n-1,2n}$ and $h_{2n,2n+1}$, respectively. $\Delta\tau = \tau_{i+1} - \tau_i = \beta_0$ and $\beta = M\beta_0$.

matrix:

$$\begin{aligned} Z = \mathrm{Tr}\,\mathrm{e}^{-\beta H} &= \lim_{M\to\infty} \mathrm{Tr}\,(\mathrm{e}^{-\beta H_{\rm odd}/M}\mathrm{e}^{-\beta H_{\rm even}/M})^M \\ &= \lim_{M\to\infty} \mathrm{Tr}\left[\prod_{n=1}^{N/2}(\mathrm{e}^{-\beta h_{2n-1,2n}/M})\prod_{n=1}^{N/2}(\mathrm{e}^{-\beta h_{2n,2n+1}/M})\right]^M \\ &= \lim_{M\to\infty} \mathrm{Tr}\left[\prod_{n=1}^{L/2}\mathcal{T}_n(M)\right] \end{aligned} \tag{12}$$

the thermodynamic properties of $L \to \infty$ are determined by the maximum eigenvalue and its eigenvectors. To obtain the eigenvalue and the eigenvectors for a large Trotter number M, we iteratively increase the size of the quantum transfer matrix using a similar algorithm to that of the zero-temperature DMRG method.

We first represent the quantum transfer matrix as

$$\mathcal{T}_{(M)} = \begin{cases} \mathcal{T}^A_{(M)}\mathcal{T}^B_{(M)} & \text{for } M \text{ even} \\ \mathcal{T}^{A'}_{(M)}\mathcal{T}^{B'}_{(M)} & \text{for } M \text{ odd.} \end{cases} \tag{13}$$

Thus the transfer matrix for $M = 2$ is

$$\begin{aligned} &\mathcal{T}_{(M=2)}(\sigma_{2n-1,\tau_1}\sigma_{2n-1,\underline{\tau_1}}\sigma_{2n-1,\tau_2}\sigma_{2n-1,\underline{\tau_2}};\, \sigma_{2n+1,\tau_1}\sigma_{2n+1,\underline{\tau_1}\sigma_{2n+1,\tau_2}\sigma_{2n+1,\underline{\tau_2}}}) \\ &\quad = \sum_{\sigma_{2n,\tau_1}}\sum_{\sigma_{2n,\tau_2}} \mathcal{T}^A_{(M=2)}(\sigma_{2n-1,\tau_1}\sigma_{2n-1,\underline{\tau_1}}\sigma_{2n,\tau_2};\, \sigma_{2n,\tau_1}\sigma_{2n+1,\underline{\tau_1}}\sigma_{2n+1,\tau_2}) \\ &\qquad \times \mathcal{T}^B_{(M=2)}(\sigma_{2n-1,\tau_2}\sigma_{2n-1,\underline{\tau_2}}\sigma_{2n,\tau_1};\, \sigma_{2n,\tau_2}\sigma_{2n+1,\underline{\tau_2}}\sigma_{2n+1,\tau_1}). \end{aligned} \tag{14}$$

Here we have introduced $\mathcal{T}^A_{(M=2)}$ and $\mathcal{T}^B_{(M=2)}$ which are defined as

$$\begin{aligned} &\mathcal{T}^A_{(M=2)}(\sigma_{2n-1,\tau_1}\sigma_{2n-1,\underline{\tau_1}}\sigma_{2n,\tau_2};\, \sigma_{2n,\tau_1}\sigma_{2n+1,\underline{\tau_1}}\sigma_{2n+1,\tau_2}) \\ &\quad = \sum_{\sigma_{2n,\underline{\tau_1}}} \langle\sigma_{2n-1,\tau_1}\sigma_{2n-1,\underline{\tau_1}}|\mathrm{e}^{-\beta h_{\rm odd}/M}|\sigma_{2n,\tau_1}\sigma_{2n,\underline{\tau_1}}\rangle \\ &\qquad \times \langle\sigma_{2n,\underline{\tau_1}}\sigma_{2n,\tau_2}|\mathrm{e}^{-\beta h_{\rm even}/M}|\sigma_{2n+1,\underline{\tau_1}}\sigma_{2n+1,\tau_2}\rangle \end{aligned} \tag{15}$$

$$\mathcal{T}^B_{(M=2)}(\sigma_{2n-1,\tau_2}\sigma_{2n-1,\underline{\tau_2}}\sigma_{2n,\tau_1};\, \sigma_{2n,\tau_2}\sigma_{2n+1,\underline{\tau_2}}\sigma_{2n+1,\tau_1})$$

$$= \sum_{\sigma_{2n,\tau_{\underline{2}}}} \langle \sigma_{2n-1,\tau_2}\sigma_{2n-1,\tau_{\underline{2}}}|\mathrm{e}^{-\beta h_{\mathrm{odd}}/M}|\sigma_{2n,\tau_2}\sigma_{2n,\tau_{\underline{2}}}\rangle$$
$$\times \langle \sigma_{2n,\tau_{\underline{2}}}\sigma_{2n,\tau_1}|\mathrm{e}^{-\beta h_{\mathrm{even}}/M}|\sigma_{2n+1,\tau_{\underline{2}}}\sigma_{2n+1,\tau_1}\rangle \tag{16}$$

where $h_{\mathrm{odd}} = h_{2n-1,2n}$ and $h_{\mathrm{even}} = h_{2n,2n+1}$. Then we iteratively increase M of $\mathcal{T}^A_{(M)}$ and $\mathcal{T}^B_{(M)}$ as follows:

$$\mathcal{T}^A_{(M)}\mathrm{e}^{-\beta_0 h_{\mathrm{odd}}} \to \mathcal{T}^{A'}_{(M+1)} \tag{17}$$
$$\mathrm{e}^{-\beta_0 h_{\mathrm{even}}}\mathcal{T}^B_{(M)} \to \mathcal{T}^{B'}_{(M+1)} \tag{18}$$
$$\mathcal{T}^{A'}_{(M)}\mathrm{e}^{-\beta_0 h_{\mathrm{even}}} \to \mathcal{T}^{A}_{(M+1)} \tag{19}$$
$$\mathrm{e}^{-\beta_0 h_{\mathrm{odd}}}\mathcal{T}^{B'}_{(M)} \to \mathcal{T}^{B}_{(M+1)}. \tag{20}$$

An example for the increase of M, equations (17) and (18), for $M = 2$ is shown graphically in figure 5.

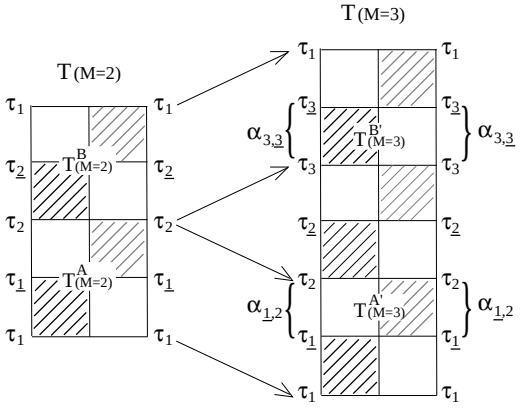

Figure 5. The increasing of M for the quantum transfer matrix $\mathcal{T}$. The $\alpha_{n,m}$ are the indices of the new basis states.

In order to represent the transfer matrix in terms of a restricted number of basis states, we have to select the important basis states which have significant weight for the representation of the transfer matrix. For this purpose we use a generalized asymmetric density matrix similar to that used in the zero-temperature DMRG method. For example, the density matrix which we use in the procedure of equation (17) for $M = 2$ is

$$\rho(\sigma_{2n-1,\tau_{\underline{1}}}\sigma_{2n-1,\tau_2};\, \sigma_{2n+1,\tau_{\underline{1}}}\sigma_{2n+1,\tau_2})$$
$$= \sum_{\sigma_{\tau_1}}\sum_{\sigma_{\tau_{\underline{2}}}} V^L(\sigma_{\tau_1}\sigma_{2n-1,\tau_{\underline{1}}},\, \sigma_{2n-1,\tau_2}\sigma_{\tau_{\underline{2}}} j V^R i \sigma_{\tau_1}\sigma_{2n+1,\tau_{\underline{1}}},\, \sigma_{2n+1,\tau_2}\sigma_{\tau_{\underline{2}}}) \tag{21}$$

where V^L and V^R are the left and right eigenvectors of $\mathcal{T}_{(M=2)}$ which have the maximum eigenvalue. The V^L and V^R are generally different owing to the transfer matrix being non-Hermitian. The diagonalization of the density matrix provides eigenvectors, v^L_α and v^R_α, which satisfy the equations

$$\sum_{\sigma_{\tau_{\underline{1}}}\sigma_{\tau_2}} v^L_\alpha(\sigma_{\tau_{\underline{1}}}\sigma_{\tau_2})\rho(\sigma_{\tau_{\underline{1}}}\sigma_{\tau_2};\, \sigma'_{\tau_{\underline{1}}}\sigma'_{\tau_2}) = \gamma_\alpha v^L_\alpha(\sigma'_{\tau_{\underline{1}}}\sigma'_{\tau_2}) \tag{22}$$
$$\sum_{\sigma_{\tau_{\underline{1}}}\sigma_{\tau_2}} \rho(\sigma'_{\tau_{\underline{1}}}\sigma'_{\tau_2};\, \sigma_{\tau_{\underline{1}}}\sigma_{\tau_2}) v^R_\alpha(\sigma_{\tau_{\underline{1}}}\sigma_{\tau_2}) = \gamma_\alpha v^R_\alpha(\sigma'_{\tau_{\underline{1}}}\sigma'_{\tau_2}). \tag{23}$$

We select the m eigenvectors which have the largest eigenvalues γ_α, and we use them as the new basis states:

$$\langle\alpha_{2n-1}| = \sum_{\sigma_{2n-1,\tau_{\underline{1}}}} \sum_{\sigma_{2n-1,\tau_2}} v_\alpha^L(\sigma_{2n-1,\tau_{\underline{1}}}\sigma_{2n-1,\tau_2})\langle\sigma_{2n-1,\tau_{\underline{1}}}\sigma_{2n-1,\tau_2}| \tag{24}$$

$$|\alpha_{2n+1}\rangle = \sum_{\sigma_{2n+1,\tau_{\underline{1}}}} \sum_{\sigma_{2n+1,\tau_2}} v_\alpha^R(\sigma_{2n+1,\tau_{\underline{1}}}\sigma_{2n+1,\tau_2})|\sigma_{2n+1,\tau_{\underline{1}}}\sigma_{2n+1,\tau_2}\rangle. \tag{25}$$

Then we represent $\mathcal{T}^{A'}_{(M=3)}$ as

$$\begin{aligned}\mathcal{T}^{A'}_{(M=3)}&(\sigma_{2n-1,\tau_1}\alpha_{2n-1,\tau_{\underline{1},2}}\sigma_{2n-1,\tau_{\underline{2}}};\sigma_{2n,\tau_1}\alpha'_{2n+1,\tau_{\underline{1},2}}\sigma_{2n,\tau_{\underline{2}}})\\ &= \sum_{\sigma_{2n-1,\tau_{\underline{1}}}}\sum_{\sigma_{2n-1,\tau_2}}\sum_{\sigma_{2n+1,\tau_{\underline{1}}}}\sum_{\sigma_{2n+1,\tau_2}}\sum_{\sigma_{2n,\tau_2}} v_\alpha^R(\sigma_{2n-1,\tau_{\underline{1}}}\sigma_{2n-1,\tau_2})v_{\alpha'}^L(\sigma_{2n+1,\tau_{\underline{1}}}\sigma_{2n+1,\tau_2})\\ &\times \mathcal{T}^A_{(M=2)}(\sigma_{2n-1,\tau_1}\sigma_{2n-1,\tau_{\underline{1}}}\sigma_{2n,\tau_2};\sigma_{2n,\tau_1}\sigma_{2n+1,\tau_{\underline{1}}}\sigma_{2n+1,\tau_2})\\ &\times \langle\sigma_{2n-1,\tau_2}\sigma_{2n-1,\tau_{\underline{2}}}|\mathrm{e}^{-\beta h_{\mathrm{odd}}/M}|\sigma_{2n,\tau_2}\sigma_{2n,\tau_{\underline{2}}}\rangle.\end{aligned} \tag{26}$$

We repeat a similar procedure for equations (17) to (26), and obtain the maximum eigenvalue and its eigenvectors of the quantum transfer matrix for a desired M.

Compared with the zero-temperature DMRG algorithm, the finite-T DMRG method is more subtle from the point of view of numerical stability. The asymmetric density matrix sometimes yields complex eigenvalues, although in principle they must be real. To avoid such unphysical complex eigenvalues, we need accurate numerical calculations taking account of the various symmetries of the system.

The free energy per site for the infinite system is obtained from the maximum eigenvalue λ of the transfer matrix as $F = -(T/2)\ln\lambda$. Static quantities such as the specific heat and the susceptibilities are obtained from the free energy. The specific heat is calculated by taking the numerical derivatives of F with respect to the temperature T. The spin and charge susceptibilities are calculated by means of a shift of F under an applied magnetic field or chemical potential.

The calculation of the dynamic quantities requires additional steps. We first calculate correlation functions in the β-direction. This calculation requires good accuracy for the eigenvectors of the transfer matrix $\langle\Psi^L|$ and $|\Psi^R\rangle$. Thus it is necessary to use the finite-system algorithm of the DMRG method. The Green's function in the β-direction is obtained from the left and the right eigenvectors of the transfer matrix whose eigenvalue is the largest (see figure 6):

$$G(\tau_j) \equiv -\mathrm{Tr}\{\mathrm{e}^{-\beta H}c_{i\sigma}(\tau_j)c^\dagger_{i\sigma}(0)\}/Z = -\langle\Psi^L|c_{i\sigma}(\tau_j)c^\dagger_{i\sigma}(0)|\Psi^R\rangle. \tag{27}$$

Similarly a local dynamic correlation function $\chi_{AB}(\tau_j)$ is obtained as

$$\chi_{AB}(\tau_j) \equiv \mathrm{Tr}\{\mathrm{e}^{-\beta H}A_i(\tau_j)B_i(0)\}/Z = \langle\Psi^L|A_i(\tau_j)B_i(0)|\Psi^R\rangle. \tag{28}$$

By Fourier transformation, the Green's function and the dynamic correlation function as functions of the imaginary frequencies are obtained as

$$G(\mathrm{i}\omega_n) = \frac{\beta}{M}\sum_j \mathrm{e}^{\mathrm{i}\omega_n\tau_j}G(\tau_j), \tag{29}$$

$$\chi_{AB}(\mathrm{i}\omega_n) = \frac{\beta}{M}\sum_j \mathrm{e}^{\mathrm{i}\omega_n\tau_j}\chi_{AB}(\tau_j) \tag{30}$$

where ω_n is the Matsubara frequency that is $\pi(2n+1)/\beta$ for fermionic operators and $2\pi n/\beta$ for bosonic operators.

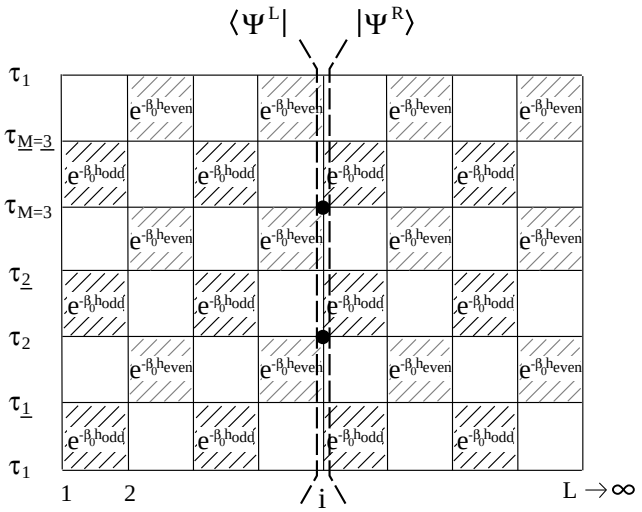

Figure 6. A schematic diagram of the calculation of the imaginary-time correlation function $\langle\Psi^L|c_{i\sigma}(\tau_3)c^\dagger_{i\sigma}(\tau_2)|\Psi^R\rangle$. The Trotter number of this example is $M = 3$.

The real-frequency Green's function and the dynamic susceptibility are obtained by analytic continuation to the real-frequency axis. We can use the Padé approximants or the maximum-entropy method for this purpose. The former method is based on the fittings of $G(\mathrm{i}\omega_n)$ or $\chi_{AB}(\mathrm{i}\omega_n)$ with rational functions of the frequency $\mathrm{i}\omega_n$ which are analytically continued to the real axis via $\mathrm{i}\omega_n \to \omega + \mathrm{i}\delta$.

The maximum-entropy method is based on the spectral representations

$$G(\tau) = \int_{-\infty}^{\infty} \rho(\omega) \frac{\mathrm{e}^{-\tau\omega}}{1 + \mathrm{e}^{-\beta\omega}}\, \mathrm{d}\omega \tag{31}$$

$$\chi_{AB}(\tau) = \int_{-\infty}^{\infty} \frac{1}{\pi} \operatorname{Im}\chi_{AB}(\omega) \frac{\mathrm{e}^{-\tau\omega}}{1 - \mathrm{e}^{-\beta\omega}}\, \mathrm{d}\omega \tag{32}$$

with

$$\rho(\omega) = -\frac{1}{\pi} \operatorname{Im} G(\omega + \mathrm{i}\delta)$$

being the density of states. Starting from a flat spectrum, this method finally finds the optimal $\rho(\omega)$ and $\chi_{AB}(\omega)$ that reproduce $G(\tau)$ and $\chi_{AB}(\tau)$ best.

The dynamical structure factor $S_{AB}(\omega)$ is related to the imaginary part of $\chi_{AB}(\omega)$ through the fluctuation dissipation theorem:

$$\operatorname{Im}\chi_{AB}(\omega) = \pi(1 - \mathrm{e}^{-\beta\omega}) S_{AB}(\omega). \tag{33}$$

In section 3 we use the standard zero-temperature DMRG method to study the ground-state properties of the paramagnetic metallic phase. In section 4 after a brief discussion of the ground-state properties, using the zero-temperature DMRG method, finite-temperature properties of the Kondo spin-liquid phase will be discussed extensively, using the finite-T DMRG method.

3. Tomonaga–Luttinger liquid properties of the paramagnetic metallic phase

This section is concerned with the paramagnetic phase away from half-filling; see figure 1. Since there is no symmetry breaking, it is natural to consider that away from half-filling the translationally invariant Kondo lattice model is metallic. In one dimension it is well known that various interacting metallic systems including the Hubbard model and the t–J model belong to the universality class of Tomonaga–Luttinger liquids [11]. Therefore, the first question concerning the paramagnetic metallic phase of the Kondo lattice model is whether it belongs to this class or not [12, 13, 4].

The spin-1/2 Tomonaga–Luttinger liquids have gapless charge and spin excitations. In one dimension the charge excitations are characterized by the velocity of the charge density v_ρ and the correlation exponent K_ρ. Similarly, the spin excitations are characterized by the velocity of the spin density v_σ, but the correlation exponent in the spin sector is fixed by the SU(2) symmetry, $K_\sigma = 1$. The low-energy physics of a Tomonaga–Luttinger liquid is completely determined when these parameters are obtained. For example, the spin and charge susceptibilities are given by

$$\chi_\sigma = \frac{2}{\pi v_\sigma} \tag{34}$$

$$\chi_\rho = \frac{2K_\rho}{\pi v_\rho}. \tag{35}$$

Reflecting the gapless excitations, the density–density and spin–spin correlation functions show power-law decays where the exponents are determined by the correlation exponent, K_ρ. The asymptotic forms of the density–density and spin–spin correlation functions are

$$\langle n(x)n(0)\rangle = K_\rho/(\pi x)^2 + A_1\cos(2k_{\mathrm{F}}x)x^{-(1+K_\rho)} + A_2\cos(4k_{\mathrm{F}}x)x^{-4K_\rho} \tag{36}$$

$$\langle S(x)S(0)\rangle = 1/(\pi x)^2 + B_1\cos(2k_{\mathrm{F}}x)x^{-(1+K_\rho)} \tag{37}$$

where $k_{\mathrm{F}} = \pi\rho/2$, with ρ being the density of charge carriers, is the Fermi momentum [14]. The logarithmic corrections are omitted in equations (36) and (37).

For the Hubbard model or the t–J model, the definition of the density of carriers is straightforward. On the other hand, for the Kondo lattice model it is already questionable. When we naively take the conduction electrons as carriers, then the Fermi momentum is given by $k_{\mathrm{F}} = k_{\mathrm{F}s} = \pi n_{\mathrm{c}}/2$. However, a different point of view is possible. Let us consider the Kondo lattice model as an effective Hamiltonian for the periodic Anderson model. For the latter, the density of carriers is the sum of the f-electron density and the conduction electron density. According to the Luttinger sum rule [1], the positioning of Fermi points does not change when the interaction is increased as long as the ground state remains paramagnetic. Therefore this property may be carried over to the Kondo lattice model and it would also be natural to assume that $k_{\mathrm{F}} = k_{\mathrm{F}l} = \pi(1 + n_{\mathrm{c}})/2$ for the Kondo lattice model [15, 12, 16, 13].

As regards the paramagnetic metallic phase, there are two basic questions.

(a) Is it a Tomonaga–Luttinger liquid?
(b) If it is, what is the size of the Fermi momentum? Is it large, $k_{\mathrm{F}l} = \pi(1 + n_{\mathrm{c}})/2$, or small, $k_{\mathrm{F}s} = \pi n_{\mathrm{c}}/2$?

The DMRG method is a powerful method for addressing these questions.

Let us denote the ground-state energy in a given spin-S subspace for a finite system with L sites by $E_g(L, N_{\mathrm{c}}, S)$ where N_{c} is the number of conduction electrons. In the following we will consider only even L and N_{c}, and thereby integer S. The spin gap of a finite system is defined by

$$\Delta_s(L) = E_g(L, N_{\mathrm{c}}, S = 1) - E_g(L, N_{\mathrm{c}}, S = 0). \tag{38}$$

As regards the charge excitations, we study the difference of the chemical potentials, $\mu_+ - \mu_-$, which is given by

$$2\mu_+ = E_g(L, N_c + 2, S = 0) - E_g(L, N_c, S = 0) \tag{39}$$

$$2\mu_- = E_g(L, N_c - 2, S = 0) - E_g(L, N_c, S = 0). \tag{40}$$

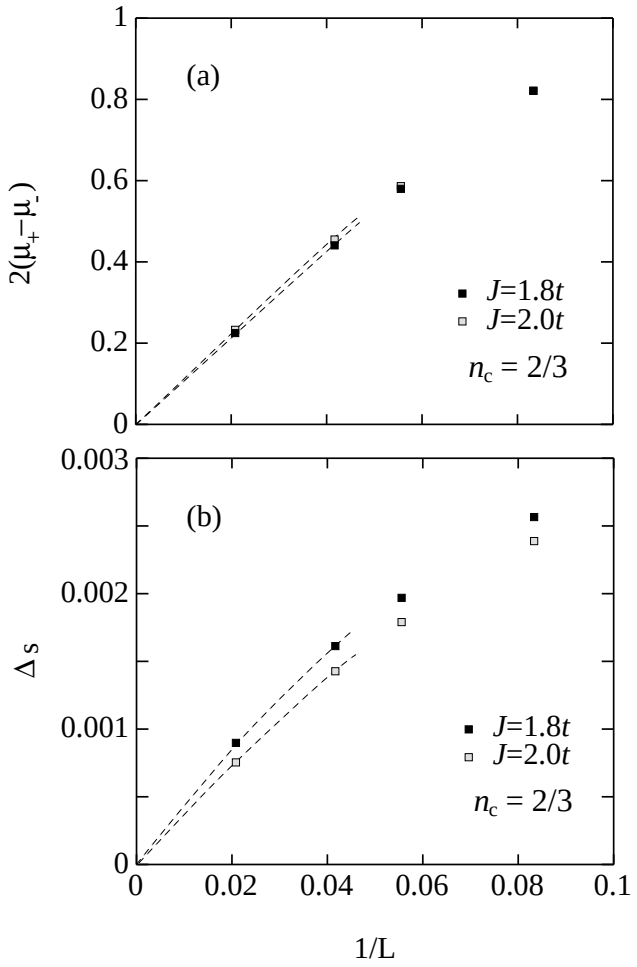

Figure 7. (a) The size dependence of the difference of the chemical potentials, $\mu_+ - \mu_-$, in the one-dimensional Kondo lattice model. (b) The size dependence of the spin gap. L is the system size, and the density of conduction electrons is fixed at $n_c = 2/3$. The energy unit is t. Typical truncation errors in the DMRG calculations are 10^{-4}.

Figure 7 shows (a) the spin-excitation gap and (b) the difference of the chemical potentials as a function of the inverse of the system size. For the example, the density of the conduction electrons is fixed at $n_c = 2/3$ [13]. Both quantities go to zero as $1/L \to 0$, which means that the spin excitations and the charge excitations are gapless. Therefore it is most likely that the paramagnetic metallic phase of the Kondo lattice model belongs to the universality class of the Tomonaga–Luttinger liquids.

Now we will determine the parameters of the Tomonaga–Luttinger liquid. From the slope

Table 1. Luttinger liquid parameters of the one-dimensional Kondo lattice model. The carrier density n_c is 2/3. The energy unit is t. The errors are estimated from the ambiguity of the power-law decay of the charge-density Friedel oscillations.

	K_ρ	v_σ	χ_σ	v_ρ	χ_ρ
$J/t = 0$	1	—	—	1.73	0.37
$J/t = 1.5$	0.19 ± 0.03			0.30 ± 0.06	0.42
$J/t = 1.8$	0.24 ± 0.02	0.014	46	0.41 ± 0.06	0.38
$J/t = 2.0$	0.27 ± 0.02	0.011	56	0.48 ± 0.06	0.36

of the spin gap, the velocities of the spin excitations are determined by

$$\Delta_s(L) = v_\sigma \pi / L \tag{41}$$

since the lowest spin excitation of a finite system with open boundary conditions has the wavenumber π/L. The difference of the chemical potentials is related to the charge susceptibility by

$$\mu_+ - \mu_- = \frac{2}{\chi_\rho L}. \tag{42}$$

The values in table 1 for v_σ and χ_ρ are determined from the slopes. The values of the spin susceptibility in table 1 are obtained from the spin velocity through equation (34).

To determine the charge velocity and the correlation exponent separately, another independent measurement is necessary. The correlation exponent K_ρ may be determined from the density–density or the spin–spin correlation functions. However, determination of the exponent of a power-law decay is the most difficult part of any numerical calculations. In order to determine K_ρ, we need to find the long-range behaviours of the correlation functions with sufficient accuracy. Instead of looking at the correlation functions, we looked at the Friedel oscillations, because the latter are numerically more reliable than the former [13, 17]. The reason for this is that the correlation functions are site off-diagonal, while the Friedel oscillations are site diagonal.

The Friedel oscillations are density oscillations induced by a local perturbation. In a Tomonaga–Luttinger liquid, power-law anomalies in the correlation functions are naturally reflected in the Friedel oscillations. The usual Friedel oscillations induced by an impurity potential are given by

$$\delta\rho(x) \sim C_1 \cos(2k_F x) x^{(-1-K_\rho)/2} + C_2 \cos(4k_F x) x^{-2K_\rho} \tag{43}$$

as a function of the distance x from the impurity [18–20]. Analogously, spin-density oscillations induced by a local magnetic field behave as

$$\sigma(x) \sim D_1 \cos(2k_F x) x^{-K_\rho}. \tag{44}$$

Thus, we can determine K_ρ from the asymptotic form of the oscillations. It is worth noting that the origin of the RKKY interaction may be traced back to the spin-density oscillations induced by a localized spin.

The charge-density oscillations induced by the open boundary conditions are shown in figure 8 for $J = 1.5t$ and $J = 2.5t$ at the density $n_c = 4/5$ [17]. The spin-density oscillations induced by the local magnetic fields applied at both ends in opposite directions are shown in figure 9 for the same set of parameters [17]. It is clearly seen that the dominant period of the charge-density oscillations is five sites, $q = 2\pi/5$, while for the spin-density oscillations it is ten sites, $q = \pi/5$.

In the strong-coupling limit of the Kondo lattice model, each conduction electron forms a local singlet with the f spin at the same site. However, away from half-filling these singlets

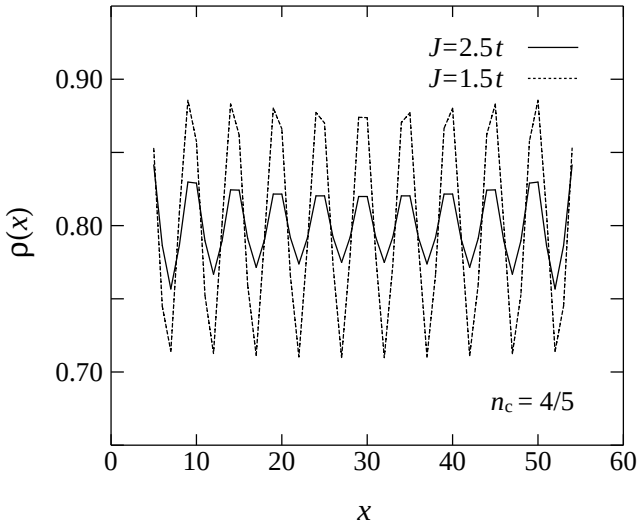

Figure 8. Charge-density oscillations of the Kondo lattice model. The system size is 60 sites and the carrier density is $n_c = 4/5$. The solid line and the broken line correspond to $J = 2.5t$ and $J = 1.5t$, respectively. Typical truncation errors in the DMRG calculations are 1×10^{-6} for $J = 2.5t$ and 3×10^{-6} for $J = 1.5t$.

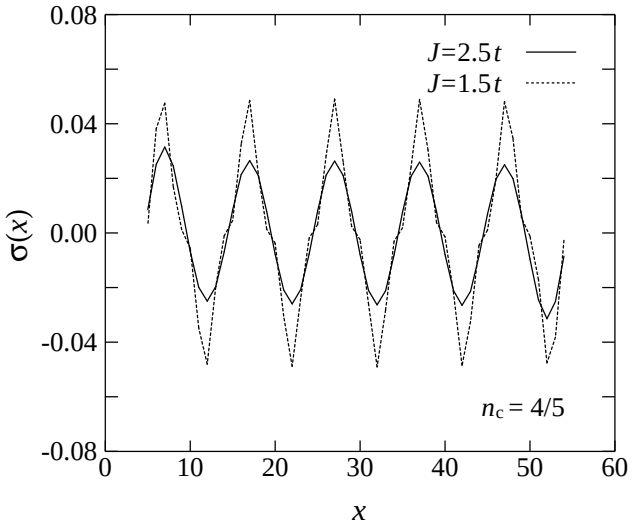

Figure 9. Spin-density oscillations of the Kondo lattice model. The system size is 60 sites and the carrier density is $n_c = 4/5$. The solid line and the broken line correspond to $J = 2.5t$ and $J = 1.5t$, respectively. The strength of the local magnetic field h is $0.1t$. Typical truncation errors in the DMRG calculations are 1×10^{-6} for $J = 2.5t$ and 3×10^{-6} for $J = 1.5t$.

can move in the lattice with the elements of the effective hopping matrix reduced by half. Equivalently, we can regard the unpaired f spins as mobile objects with the reduced hopping energy $t/2$ with its sign reversed. Note that in the original model, hopping matrix elements are defined by $-t$. Thus the effective model of the strong-coupling limit is the t-model where the number of carriers is $L - N_c$ and double occupancy of the carriers is prohibited.

The charge response of the system is identical to that of the spinless fermions where the Fermi point is given by $\pi - \pi(1 - n_c) = \pi n_c$. Therefore the induced charge density shows oscillations corresponding to $2\pi n_c$, which is equivalent to $4k_{Fs}$ and $4k_{Fl}$. This analysis shows that in the strong-coupling limit the amplitude of the $4k_F$-oscillations dominates over the $2k_F$-oscillations for the charge Friedel oscillations, equation (43). The period of five sites is naturally understood in this way and we have confirmed that for a weaker coupling the amplitude of the $2k_F$-oscillation develops.

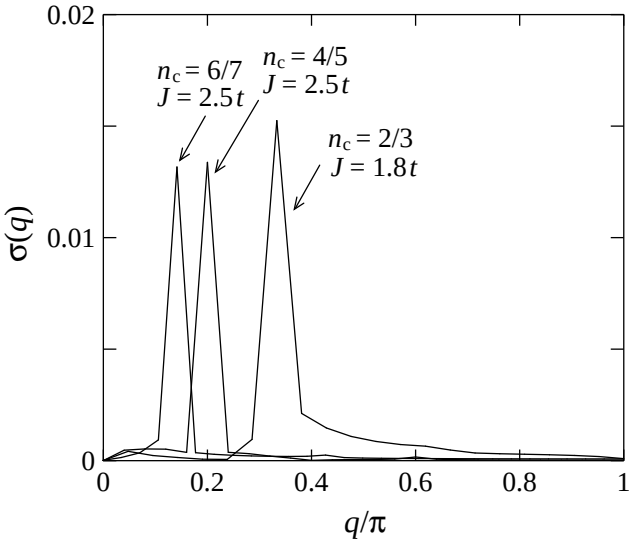

Figure 10. Fourier components of the spin-density Friedel oscillations.

When we consider the spins of the unpaired f electrons, there remains a macroscopic 2^{L-N_c}-fold degeneracy. For the spin sector, the lifting of the degeneracy is essential. For the specific model where the degeneracy is lifted by the next-nearest-neighbour hoppings, it is shown analytically that the Fermi surface is big, $k_F = k_{Fl}$ [12]. For a finite J, the degeneracy of the Kondo lattice model is always lifted. The period of ten sites of the spin-density Friedel oscillations shown in figure 9 indicates that the $2k_F$-oscillations corresponding to $2k_{Fl}$ are actually observed. Figure 10 shows that the $2k_{Fl}$-oscillations corresponding to the large Fermi surface are always dominating in the paramagnetic phase for various coupling constants and various densities.

The Friedel oscillations obtained by the DMRG method clearly indicate that the Fermi surface of the Kondo lattice model is large. At the early stage, the conclusions of the bosonization studies were controversial. In the area of the paramagnetic metallic phase, Fujimoto and Kawakami obtained the Tomonaga–Luttinger liquid with a large Fermi surface, while White and Affleck predicted a Luther–Emery liquid with a spin gap [21, 22]. Later, it was argued that an additional direct Heisenberg coupling between the f spins is necessary to stabilize the Luther–Emery liquid [23]. Furthermore, the existence of a gapless excitation with the momentum of $2k_{Fl}$ is shown rigorously by the Lieb–Schultz–Mattis construction [24].

In order to obtain the correlation exponent K_ρ, we used the slope of the envelope function of the charge-density oscillations, assuming that the dominant component of the oscillations is the $4k_F$-oscillations. Figure 11 shows K_ρ thus determined for the exchange coupling constants from $J = 4.0t$ to $1.5t$. The density of the conduction electrons is fixed at $n_c = 2/3$. K_ρ is

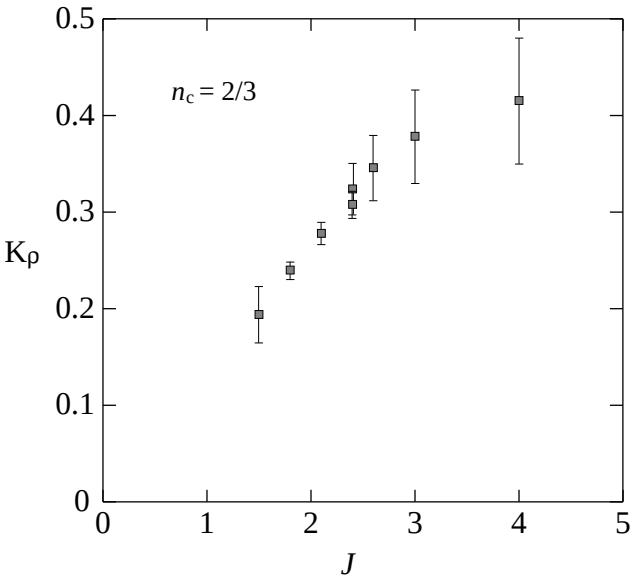

Figure 11. The correlation exponent K_ρ estimated from the decay rate of the charge-density Friedel oscillations. The error bars are estimated from the ambiguity of the power-law fitting. $n_c = 2/3$. J is in units of t.

always smaller than 1/2 and monotonically decreases with decreasing J. The limiting value of $K_\rho = 1/2$ in the strong-coupling limit is easy to understand since the strong-coupling limit of the Kondo lattice model is equivalent to the $U = \infty$ Hubbard model.

The correlation exponent shows a small discontinuity at the boundary between the ferromagnetic and the paramagnetic phases, $J_c = 2.4t$ [4, 25–27] for $n_c = 2/3$. Below J_c, K_ρ decreases more quickly and becomes lower than 1/3, which means that the long-range behaviour of the density–density correlation is governed by the $4k_F$-oscillations rather than the $2k_F$-oscillations. With further decreasing J, K_ρ seems to cross the value $3 - 2\sqrt{2} \sim 0.17$. Since the exponent of the power-law anomaly of the momentum distribution function is given by $(K_\rho + 1/K_\rho - 2)/4$, the power-law anomaly is removed below this point and a clear Fermi surface cannot be seen any longer. K_ρ seems to monotonically decrease toward 0 with J approaching the singular point $J = 0$.

Through the study of the Friedel oscillations by the DMRG method, it has become clear that the paramagnetic metallic phase of the one-dimensional Kondo lattice model is a Tomonaga–Luttinger liquid with a large Fermi surface. This Tomonaga–Luttinger liquid is unique in the sense that K_ρ is smaller than 1/2. This small value of K_ρ may be attributed to the long-range nature of the effective interactions with strong retardation [14, 28]. Recently, observation of the Friedel oscillations by the DMRG method has been shown to be useful also in the discussion of critical behaviours of the Hubbard model [29].

4. The Kondo spin-liquid phase at half-filling

The half-filled KL model is always insulating in one dimension. This conclusion was obtained from exact-diagonalization study [5]. On the basis of a finite-size scaling, it was shown that the finite excitation gap remains for any finite J. The result has been confirmed by the DMRG

method [30] and was later supported by a mapping to a non-linear sigma model [31] and by the bosonization approach [32]. In this section we discuss the basic properties of this insulating state.

As regards the insulating phase, the question that we would like to address here is that of which characteristics distinguish the Kondo insulators from the usual semiconductors. The most significant difference is that there are no gaps at high temperatures and they are induced as the temperature is lowered. Furthermore, the excitation gaps induced by the temperature are different according to the channels. The difference of the excitation gaps and more generally the differences between the temperature dependences of various excitation spectra are naturally reflected in the temperature dependences of various thermodynamic quantities.

Clearly the lowest excitation gap which is the spin gap for the Kondo insulator defines the smallest energy scale of the system. In ordinary band insulators the band gap defines the smallest energy scale which controls not only the spin excitations but also the charge excitations. It is also interesting to compare the smallest energy scale of the Kondo lattice problem with that of the single-impurity Kondo effect, namely the Kondo temperature T_K. It is well known that the low-temperature properties of the impurity model are governed by the single energy scale of T_K.

In the present section, first we will discuss the spin gap, the charge gap and the quasiparticle gap, using the zero-temperature DMRG method. Then we will discuss the temperature dependence of the spin susceptibility, the charge susceptibility and the specific heat, using the finite-T DMRG method. The temperature dependences of the single-particle excitation spectrum, the dynamic spin–spin correlation function and the charge–charge correlation function are also discussed using the finite-T DMRG method. For the analytic continuation which is necessary for discussing the dynamic quantities, it is shown that the maximum-entropy method is very useful [33–35].

4.1. Spin, charge and quasiparticle gaps

To understand the physics of the insulating state of the half-filled Kondo lattice model, it is instructive to consider the limit of strong exchange coupling J. In this limit every f spin, together with a conduction electron, forms a local singlet at every site. To create spin excitations, the minimum energy cost is J, which is the energy difference between the local spin-singlet state and the local spin-triplet state. On the other hand, creation of charge excitations requires the minimum energy of $3J/2$, which corresponds to the energy cost of breaking two local singlets by transferring a conduction electron to a neighbouring site.

The excitation gaps monotonically decrease with decreasing exchange constant, but they do not vanish at any finite value of J. In particular, the weak-coupling limit $J \ll t$ is interesting. In this regime the KL model is equivalent to the periodic Anderson model with strong Coulomb repulsion in the f orbitals. The salient feature of the strong Coulomb interaction in the periodic Anderson model appears in the diverging ratio between the charge and spin gaps. The limit of $J = 0$ is singular; here, the conduction electrons and the f spins are decoupled, and both the spin and charge gaps vanish.

For the discussion of the gaps, we take into account also the Coulomb interaction between the conduction electrons. Since the spin and charge gaps are tiny in the weak-coupling regime, it is no longer justified to neglect the Coulomb interaction between the conduction electrons. This Coulomb interaction suppresses the double occupation of conduction electrons, which eventually leads to the formation of local magnetic moments of the conduction electrons. Therefore the effect of the Coulomb interaction on the spin and charge gaps of the KL model sheds light on the nature of the gap formation in the Kondo insulators.

The model that we consider in this subsection is the following one-dimensional KL model with the Coulomb interaction between the conduction electrons U_c:

$$H = -t\sum_{i\sigma}(c^{\dagger}_{i\sigma}c_{i+1\sigma} + \mathrm{HC}) + J\sum_{i\mu} S^{\mu}_i\sigma^{\mu}_i + U_c\sum_i\left(c^{\dagger}_{i\uparrow}c_{i\uparrow} - \frac{1}{2}\right)\left(c^{\dagger}_{i\downarrow}c_{i\downarrow} - \frac{1}{2}\right). \tag{45}$$

The Coulomb interaction is represented in the last term. In this section we consider the case of half-filling where the total number of conduction electrons is equal to the number of lattice sites L:

$$N_c \equiv \sum_{i\sigma} c^{\dagger}_{i\sigma}c_{i\sigma} = L.$$

This Hamiltonian is reduced to the Hubbard model in the limit of $J \to 0$, and to the usual KL model for $U_c = 0$.

In the impurity Kondo model, all low-temperature properties are scaled by the single energy scale $T_K \sim D\exp(-1/\rho J)$, where ρ is the density of states of the conduction band at the Fermi level and is given by $1/2\pi t$ in one dimension. In contrast to the single-impurity Kondo model, the KL model has many f spins which are coupled through the conduction electrons. A basic question of the lattice problem is how the intersite correlations appear in the energy scale. The simplest extension of the form of T_K may be the inclusion of an enhancement factor in the exponent: the spin gap is expected to behave as

$$\Delta_s \propto \exp\left(-\frac{1}{\alpha\rho J}\right) \tag{46}$$

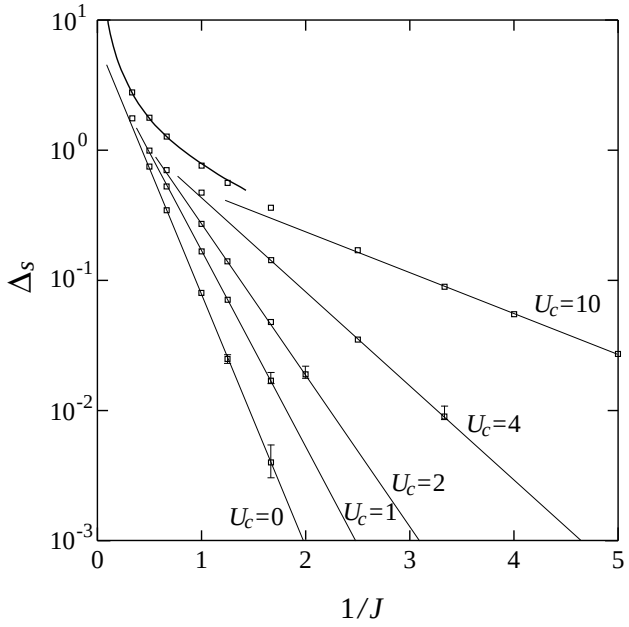

Figure 12. The spin gap of the half-filled one-dimensional Kondo lattice model with Coulomb interaction. The thick curve represents the result from perturbation theory in terms of t/J for $U_c = 10t$. A typical truncation error in the DMRG calculation is 10^{-6} for $J = 1$. The error bars are estimated from L^{-1}- and L^{-2}-scalings. The gap energies, exchange constant J and Coulomb interaction U_c are in units of t.

where α is the enhancement factor. The Gutzwiller approximation predicts the enhancement factor $\alpha = 2$ [36]. Tsunetsugu *et al* have estimated that the enhancement factor in one dimension is in the range $1 \leqslant \alpha \leqslant 5/4$ by using a finite-size scaling for the results obtained by means of exact diagonalization [5]. In the following we present the results on the enhancement factor obtained by the DMRG method.

The spin gap is obtained from the difference of the ground-state energies in the subspaces where the total S^z is zero and one, equation (38); the SU(2) symmetry in the spin space guarantees that the energy difference is the same as the spin gap in the subspace of zero total S^z. The spin gap of the bulk system is estimated from the following scaling function:

$$\Delta_s(L) = \Delta_s(\infty) + \beta L^{-2} + \mathrm{O}(L^{-4}). \tag{47}$$

The spin gaps obtained are plotted in figure 12 on a logarithmic scale as a function of $1/J$. The results are obtained by the extrapolation to the bulk limit using the data for $L = 6, 8, 12, 18, 24, 40$. The DMRG calculations were done by using the finite-system algorithm with open boundary conditions, retaining up to 300 states for each block. The enhancement factor is obtained from the slope in the figure, and determined to be $\alpha = 1.4(1)$ for $U_\mathrm{c} = 0$. There are some uncertainties in the extrapolation to the bulk limit for tiny gaps. However, within the present accuracy we do not observe any indication of the logarithmic correction to the exponent which was predicted by the semiclassical approach [31].

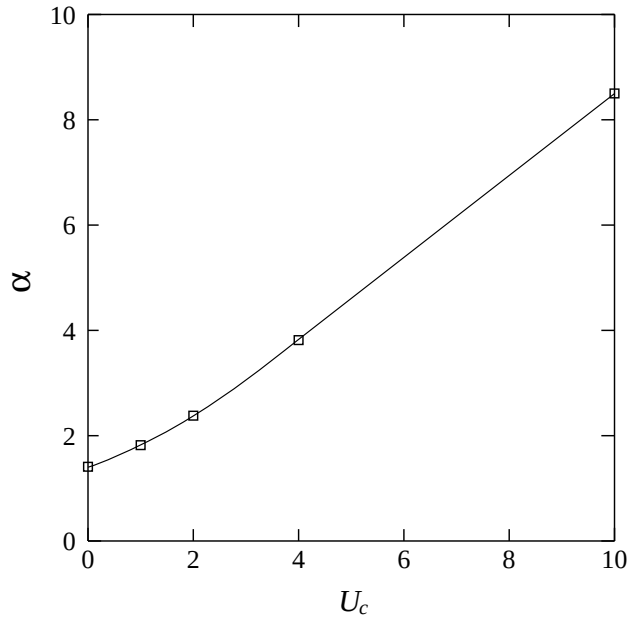

Figure 13. The U_c-dependence of the exponent of the spin gap. The Coulomb interaction U_c is in units of t.

Now we consider the effect of the Coulomb interaction. In the weak-coupling region it is natural to extend the form of equation (46) to finite U_c allowing the U_c-dependence of the exponent. Indeed the numerical data are nicely fitted by this form, as shown in figure 12. The U_c-dependence obtained is shown in figure 13, which indicates that $\alpha(U_\mathrm{c})$ increases with increasing U_c and the asymptotic behaviour is linear in U_c. The KL model with the Coulomb interaction is mapped to a Heisenberg chain coupled with the localized f spins in the limit

of $U_c/t \to \infty$. The linear U_c-dependence of the exponent $\alpha = 0.78U_c/t + 0.7$ in figure 13 means that the spin gap of the effective-spin model behaves as $\Delta_s \sim \exp(-2J_{\rm eff}/J)$ with $J_{\rm eff} = 4t^2/U_c$ being the effective coupling of the Heisenberg chain. In order to check this form, we have analysed the numerical data for the spin system obtained by Igarashi *et al* [37], and found a good coincidence. Thus we conclude that the enhancement factor α increases monotonically with increasing U_c. This is natural since the origin of the spin gap is the singlet binding between the localized spins and the conduction electrons, for which the Coulomb interaction acts favourably by suppressing the double occupancy.

In contrast to the single-impurity Kondo model, the KL model has a second energy scale that characterizes the charge excitations at low temperatures. The charge excitations keep spin quantum numbers, and the charge gap is defined by the difference between the lowest energies in the subspaces of $N_c = L$ and $N_c = L+2$: $E_g(L, N_c = L+2, S = 0) - E_g(L, N_c = L, S = 0)$. Owing to the hidden SU(2) symmetry in the charge space, the energy difference is the same as the charge-excitation gap in the subspace of the fixed number of electrons $N_c = L$ [38].

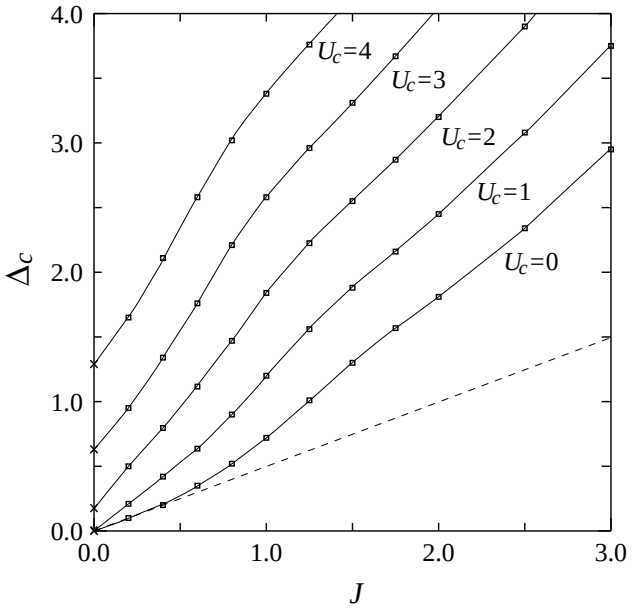

Figure 14. The charge gap of the half-filled one-dimensional Kondo lattice model with the Coulomb interaction. The results on the vertical axis were obtained from the exact solution given by Lieb and Wu. Typical truncation errors in the DMRG calculation are 10^{-6} for $J = 1$ and 10^{-4} for $J = 0.2$, which are the dominant sources of numerical errors since the finite-size scaling, equation (47), is well obeyed. The gap energies, exchange constant J and Coulomb interaction U_c are in units of t.

Figure 14 shows the charge gap obtained by the extrapolation to the infinite system. The results for $J = 0$ are known as the Hubbard gap of the one-dimensional Hubbard model which is exactly solved by the Bethe *ansatz* [39]. The asymptotic forms of the charge gap are given by $\Delta_c \propto \sqrt{U_c t}\exp(-1/\rho U_c)$ for small U_c and by $\Delta_c \propto U_c - 4t$ for large U_c. The results obtained for finite J are consistent with the exact ones, which are denoted by the crosses on the vertical axis.

For $U_c = 0$ the charge gap is linear in J in the small-J/t limit. As is shown by the exact-diagonalization study, the charge gap is much bigger than the spin gap in the weak-coupling regime [38]. This implies that the correlation length for the spin degrees of freedom

is much longer than the charge-correlation length. Therefore for the discussion of the charge gap it is justified to assume that the spin–spin correlation length is infinitely long. Under the assumption of an infinite spin-correlation length, the charge gap is calculated as

$$\Delta_c = \frac{J}{2}. \tag{48}$$

From figure 14 we also find that the charge gap increases with increasing Coulomb interaction U_c.

The charge excitations are created by adding two additional electrons, keeping the spin quantum numbers fixed. When we put a single electron in the ground state, a quasiparticle excitation is produced. Here we consider the relation between the charge gap Δ_c and the quasiparticle gap Δ_{qp}, which is defined by $E_g(L, N_c = L \pm 1, S = \pm 1/2) - E_g(L, N_c = L, S = 0)$. In the strong-coupling limit, $J/t \to \infty$, it is evident that the charge gap is twice the quasiparticle gap owing to the SU(2) symmetry in the charge space. In the second-order perturbation in t/J, one can show that the interaction between the two additional electrons is repulsive, leading only to a phase shift. Therefore the charge gap in the bulk limit is twice the quasiparticle gap Δ_{qp}:

$$\Delta_c = 2\Delta_{qp}. \tag{49}$$

A similar argument is also valid for the periodic Anderson model [38]. The validity of this relation was checked by a DMRG calculation for the entire range of the exchange constant J. As regards the spin gap, the lowest spin excitation may be considered as a bound state of a quasielectron and a quasihole.

4.2. Susceptibilities at finite temperatures

The spin and charge gaps determined at zero temperature are very different in the weak-coupling regime. The spin gap is exponentially small, while the charge gap is proportional to J. The large charge gap originates from the staggered internal magnetic fields induced by the long correlation length of the f spins. At finite temperatures, however, the spin correlations are subject to the thermal fluctuations. When the temperature becomes comparable to the spin gap, the spin-correlation length gets smaller and all of the electronic properties including the charge-excitation spectrum are reconstructed. In this section we study such an interplay between the spin and charge excitations at finite temperatures by looking at the thermodynamic quantities. In what follows, we consider the original KL model, neglecting the Coulomb interaction between the conduction electrons.

In order to calculate thermodynamic quantities, we use the finite-T DMRG method discussed in section 2 [8, 7]. In this method the free energy is obtained from the maximum eigenvalue of the quantum transfer matrix. The spin and charge susceptibilities are obtained from the derivatives of the free energy with respect to the external magnetic field or chemical potential. The calculations are performed using the infinite-system algorithm, retaining 40 states per block. The truncation errors in the calculations are typically 10^{-3} and, at the lowest temperature, 10^{-2} for the Trotter number $M = 50$.

We first consider the temperature dependence of the uniform spin susceptibility. The spin susceptibility is obtained from the change of the free energy caused by a small magnetic field h: $\delta F = \chi_s h^2/2$. The results for $J/t = 0$, 1.0, 1.2, 1.6 and 2.4 are shown in figure 15.

When $J/t = 0$, the localized spins and the conduction electrons are uncorrelated. The susceptibility is given by the sum of the Curie term due to the free f spins and the Pauli term of the free conduction electrons. The contribution of the Pauli susceptibility of the conduction

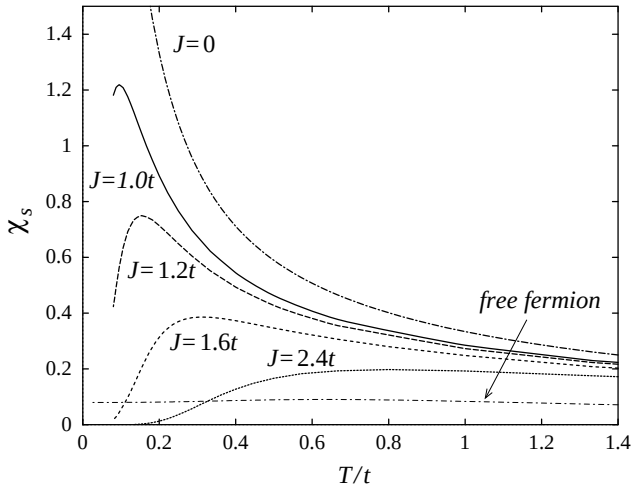

Figure 15. The spin susceptibility of the half-filled one-dimensional Kondo lattice model. The truncation errors in the finite-T DMRG calculations are typically 10^{-3} and, at the lowest temperature, 10^{-2}.

electrons shown by the dashed line in figure 15 is relatively small, and the total susceptibility for $J/t = 0$ is dominated by the Curie term.

For finite J, the low-temperature part of χ_s sharply drops with decreasing temperature. This drastic change is due to the appearance of the small energy scale for the spin sector [40, 9]. The spin gap of $0.08t$ for $J/t = 1.0$ is consistent with the characteristic temperature at which χ_s starts to decrease, deviating from the Curie law.

Table 2. Activation energies obtained from the spin and charge susceptibilities, Δ_{χ_s} and Δ_{χ_c}, of the one-dimensional Kondo lattice model at half-filling. The quasiparticle gap Δ_{qp} and the spin gap Δ_s are obtained by the zero-temperature DMRG method. The charge gap is twice the quasiparticle gap: $\Delta_c = 2\Delta_{qp}$

	Δ_{χ_s}/t	Δ_{χ_c}/t	Δ_s/t	Δ_{qp}/t
$J/t = 1.0$			0.08	0.36
$J/t = 1.2$			0.16	0.47
$J/t = 1.6$	0.45 ± 0.1	0.6 ± 0.1	0.4	0.7
$J/t = 2.4$	1.2 ± 0.1	1.0 ± 0.1	1.1	1.1
$J/t = 3.0$	1.6 ± 0.1	1.4 ± 0.1	1.8	1.5

In order to determine the energy scale at low temperatures, we estimate the activation energy by fitting the susceptibility with an exponential form. The estimated activation energy for the spin susceptibility is summarized in table 2 for $J/t = 1.6$, 2.4 and 3.0. Compared with the quasiparticle gap and the spin gap, both of which are responsible for magnetic excitations, we conclude that the lower of them determines the low-temperature energy scale of the spin susceptibility. This is consistent with the general form of the susceptibility, which is written as

$$\chi_s = Z^{-1}N^{-1}\beta \sum_m \mathrm{e}^{-\beta E_m} \langle m|S_z^{\mathrm{total}}|m\rangle^2 \tag{50}$$

$$Z = \sum_m \mathrm{e}^{-\beta E_m}. \tag{51}$$

The point is that equations (50) and (51) apply for both the canonical and the grand-canonical ensembles on properly defining the states $|m\rangle$. In the thermodynamic limit, the susceptibilities for the two ensembles should give the same answer. From this consideration it is concluded that the smaller of the spin gap and the quasiparticle gap determines the low-temperature energy scale. For the case of small exchange coupling ($J/t \ll 1$), the spin gap is smaller than the quasiparticle gap and thus the low-temperature energy scale of χ_s is determined by the spin gap.

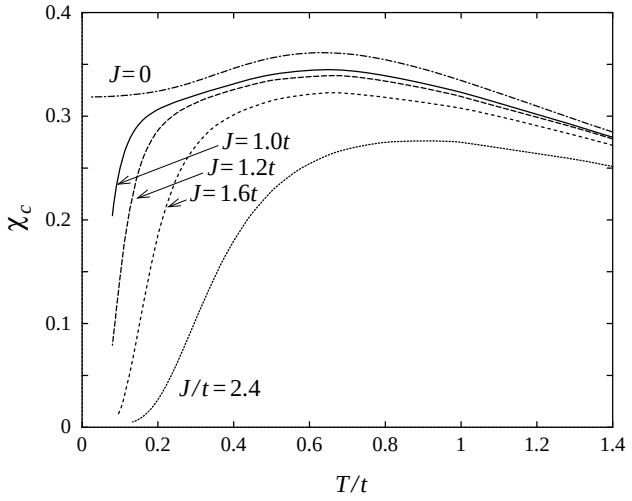

Figure 16. The charge susceptibility of the half-filled one-dimensional Kondo lattice model.

In order to see the effect of thermal fluctuations of the f spins on the charge excitations, we next calculate the charge susceptibility χ_c. χ_c is obtained from the change of the free energy due to a small shift of chemical potential μ, $\delta F = \chi_c \mu^2/2$. In the present calculation we use the fact that the chemical potential is zero at half-filling, owing to the SO(4) symmetry of the model [38]. The results for $J/t = 0$, 1.0, 1.2, 1.6 and 2.4 are shown in figure 16.

For $J/t = 0$, χ_c does not show diverging behaviour at low temperatures, in contrast to χ_s. In the limit where $T = 0$, χ_c is equal to the density of states of the conduction electrons, which is $1/\pi t$ including the two spin directions. This is expected since the charge degrees of freedom are governed by the conduction electrons. Since there is no interaction, $\chi_c/4$ is equal to the spin susceptibility of the free conduction electrons. The slight increase in χ_c in the low-temperature region is a characteristic feature of the one-dimensional system, where the density of states diverges at the band edges.

A finite value of J produces a sharp drop in χ_c at low temperatures. Similarly to the case for χ_s, this drop is due to the appearance of the small energy scale Δ_c for the charge sector. The energy scale is determined by the activation energy for the charge susceptibility. On fitting χ_c with an exponential form, the activation energy Δ_{χ_c} is obtained as listed in table 2 for $J/t = 1.6$, 2.4 and 3.0. From this table it is concluded that the quasiparticle gap determines the low-temperature energy scale of the charge susceptibility.

Although the quasiparticle gap determines the exponential temperature dependence at low temperatures, it is not the only energy scale for χ_c. This may be best understood by looking at χ_c for $J/t = 1.0$. A sharp decrease of χ_c is seen at around $T \sim 0.1t$, which is a much smaller value than that of the quasiparticle gap $0.36t$ but rather close to the value of the spin gap $0.08t$. This fact suggests that the charge-excitation spectrum is reconstructed when the temperature

is raised up to the spin gap. We will discuss this aspect in more detail in connection with the temperature dependence of various excitation spectra.

4.3. Specific heat

In order to see how the entropy of the system is released, we next calculate the specific heat. The specific heat is calculated from the second derivative of the free energy: $C = -T\,\partial^2 F/\partial T^2$. The results for $J/t = 0$, 1.0, 1.2, 1.6 and 2.4 are shown in figure 17.

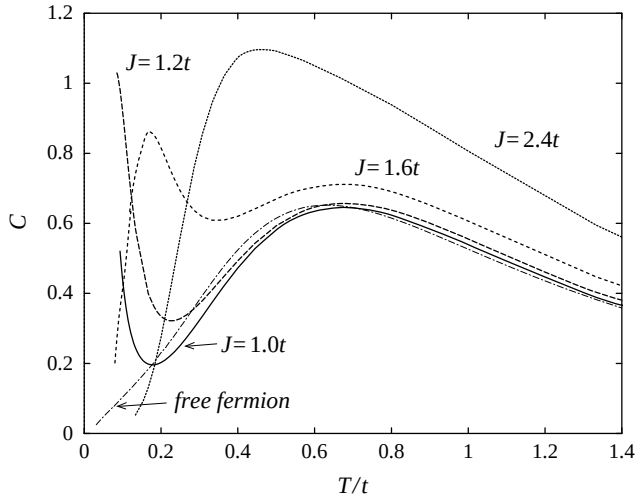

Figure 17. The specific heat of the half-filled one-dimensional Kondo lattice model.

At $J/t = 0$ the specific heat of this model is given by the sum of the contributions from the free localized spins and the free conduction electrons. For finite J they are combined to form a two-peak structure. The peak at higher temperatures is almost independent of the exchange constant and similar to the specific heat of free conduction electrons. Thus the structure at higher temperatures may be understood as a band-structure effect of the one-dimensional conduction electrons. In contrast to the higher-temperature structure, the structure at lower temperatures strongly changes its form with J. The peak shifts towards higher temperatures and becomes broader with increasing J.

With further increase of the exchange coupling, the spin gap becomes comparable to the hopping matrix element t. In this situation the various energy scales are not distinguishable and the specific heat possesses a single-peak structure as shown for $J/t = 2.4$.

4.4. Dynamic properties

The dynamic properties of the half-filled KL model show clear features characteristic of strongly correlated insulators. The unusual temperature dependence of the excitation spectra is one of the most important features of the interacting systems. In fact, the behaviour of the static susceptibilities discussed in the preceding subsection indicates that the excitation gaps develop at low temperatures.

In this section we calculate the dynamic spin and charge structure factors, $S(\omega)$ and $N(\omega)$, and the density of states, $\rho(\omega)$. By looking at their temperature dependence we can study the temperature evolution of the excitation gaps and the relations among dynamic quantities. To

obtain the dynamic quantities we first calculate the correlation functions in the imaginary-time direction. As we have discussed in section 2, the correlation functions in the imaginary-time direction are directly calculated from the left and right eigenvectors obtained by applying the finite-T DMRG method to the transfer matrix.

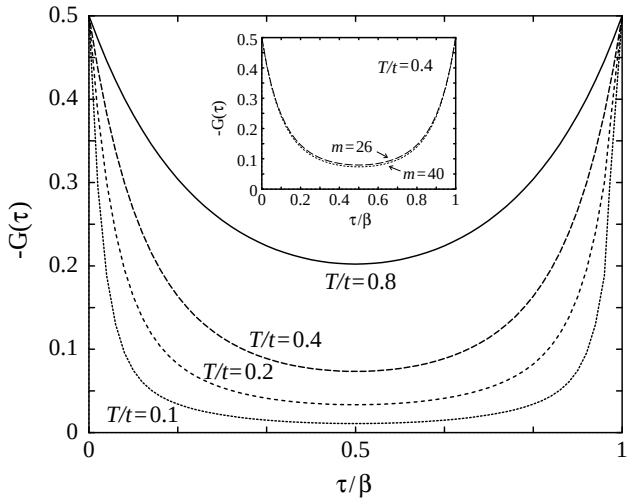

Figure 18. Imaginary-time correlation functions, $G(\tau)$, of the half-filled one-dimensional Kondo lattice model; $J/t = 1.6$. The Trotter number $M = 60$. The inset shows the results for different numbers of states, m, retained in the DMRG calculations. The truncation errors in the DMRG calculations are 2×10^{-3} for $m = 26$ and 3×10^{-4} for $m = 40$.

Examples of the single-particle Green's function as a function of the imaginary time calculated using the finite-T DMRG method are shown in figure 18. To obtain the spectral functions, we first Fourier transform the imaginary-time correlation functions and then need to perform analytic continuation from the imaginary-frequency axis to the real-frequency axis. One straightforward method for performing the analytic continuation is to use the Padé approximants. Since the DMRG calculation yields no statistical errors, the Padé approximants show good convergence in many cases. However, it is still difficult to obtain the spectral functions using the Padé approximants in a stable manner when a spectrum has a nearly singular form. The reason for this is that using the Padé approximants involves the use of rational functions of Matsubara frequencies $i\omega_n$.

Even when a spectrum has a nearly singular form, the maximum-entropy method still works well. An advantage of this method is that we can explicitly use the symmetries and the positiveness of the spectral function. The results obtained by the two methods are compared in figure 19. At high temperatures, the two sets of results coincide with each other, but with decreasing temperature the convergence of the Padé approximants becomes worse due to the growing singularity in the spectral function in the low-frequency region. The results obtained using the maximum-entropy method are stable even at low temperatures. Thus in the following we employ the maximum-entropy method to study the temperature evolution of the dynamic correlation functions [41].

The quasiparticle density of states obtained for $J/t = 1.6$ at the temperatures $T/t = 0.1$, 0.14, 0.2, 0.25, 0.3, 0.6 is shown in figure 20. The existence of the quasiparticle gap is seen as a clear dip structure around $\omega = 0$. At low temperatures sharp peaks appear at $\omega = \pm\Delta_{qp}$ separated from the higher-frequency part of the spectral weight. The sharpness of the peaks

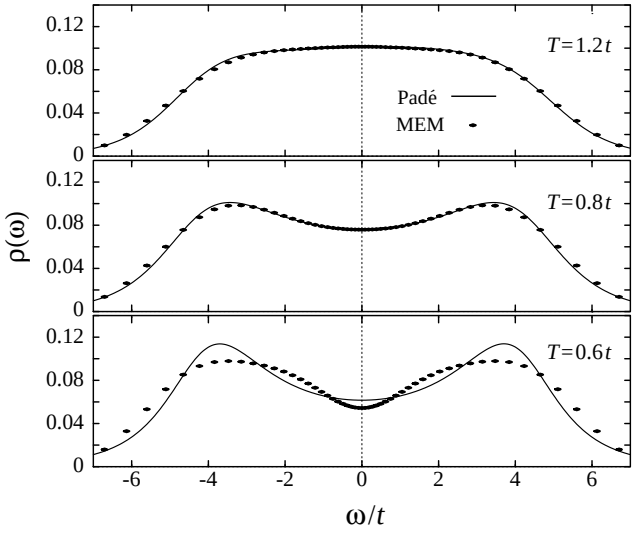

Figure 19. The quasiparticle density of states, $\rho(\omega)$, obtained from $G(\tau)$ by using the Padé approximants and the maximum-entropy method (MEM). The Trotter number $M = 60$.

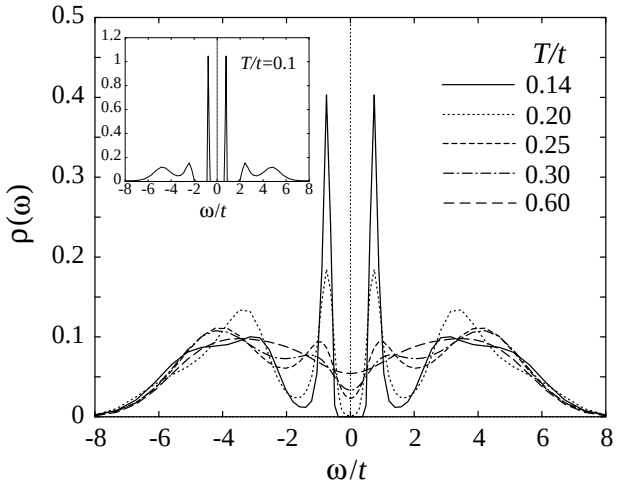

Figure 20. The quasiparticle density of states, $\rho(\omega)$, of the half-filled one-dimensional Kondo lattice model; $J/t = 1.6$. The Trotter number $M = 60$, and the number of states retained is $m = 40$.

suggests the formation of heavy-quasiparticle bands at the gap edges. The high-frequency part of the spectral weight extends to the region far from the edge of the free conduction band $\omega = 2t$, which shows the significance of the multiple excitations accompanying the quasiparticle excitations.

As the temperature is increased, the peak at the threshold gets broadened, and at the temperatures $T \sim \Delta_s$ the peak and the accompanying dip between the low- and high-frequency parts completely disappear. This result shows that although the sharp peaks of the quasiparticle density of states are located at the frequencies $\omega = \pm\Delta_{qp}$, they disappear at around the

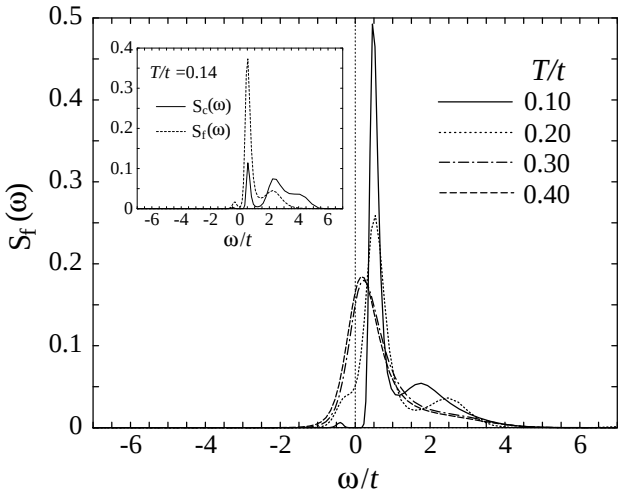

Figure 21. The dynamic spin structure factor of the f spins, $S_{\rm f}(\omega)$, in the half-filled one-dimensional Kondo lattice model; $J/t = 1.6$.

temperature $T \sim \Delta_s$ which is much lower than $T \sim \Delta_{qp}$.

In order to see what happens at the temperatures $T \sim \Delta_s$, we next consider the f-spin dynamic structure factor $S_{\rm f}(\omega)$. The calculated $S_{\rm f}(\omega)$ are presented in figure 21. At the lowest temperature the spin gap is clearly seen, with a sharp peak at the gap edge. This characteristic peak has the most of the spectral weight, which shows concentrated f-spin excitations on the energy scale of Δ_s. There is a broad peak on the higher-frequency side. As is shown later, a similar structure and temperature dependence appear in the dynamic spin structure factor of the conduction electrons $S_{\rm c}(\omega)$. Thus we conclude that through the exchange coupling, the excitations of the f spins are mixed with those of conduction spins, which yields this broad peak in the higher-frequency part of $S_{\rm f}(\omega)$.

With increasing temperature, the peak structure at $\omega = \Delta_s$ becomes broad and the spectral intensity increases around the zero frequency $|\omega| < \Delta_s$. At the temperatures $T \sim \Delta_s$, the peak position of the spectrum shifts to the zero frequency, and the peak height becomes almost temperature independent. The spectral intensity at the zero frequency is directly related to the NMR relaxation rate $1/T_1$. Hence the present results show that $1/T_1$ is nearly temperature independent at high temperatures and drastically decreases with decreasing temperature below the characteristic temperature of the order of Δ_s.

The dynamic spin structure factor for the conduction electrons, $S_{\rm c}(\omega)$, is shown in figure 22. At low temperatures, $S_{\rm c}(\omega)$ has two peaks. The peak on the low-frequency side is located at an energy of Δ_s, similarly to $S_{\rm f}(\omega)$. This peak corresponds to the spin excitations of the singlet bound states composed of conduction electrons with f spins bound to the triplet states. The high-frequency peak is located slightly above the charge gap, which corresponds to the spin excitations due to quasiparticles. With increasing temperature, both peaks lose their intensity, and above the temperature $T \sim \Delta_s$ the low-frequency peak structure disappears. The spectrum on the high-frequency side becomes similar to that of the dynamic charge structure factor $N(\omega)$. This means that high-frequency excitations are dominated by the quasiparticle excitations of almost free conduction electrons, and thus the relation $S_{\rm c}(\omega) = N_{\rm c}(\omega)/4$ is satisfied approximately.

The dynamic charge structure factor $N(\omega)$ is shown in figure 23. At the lowest temperature,

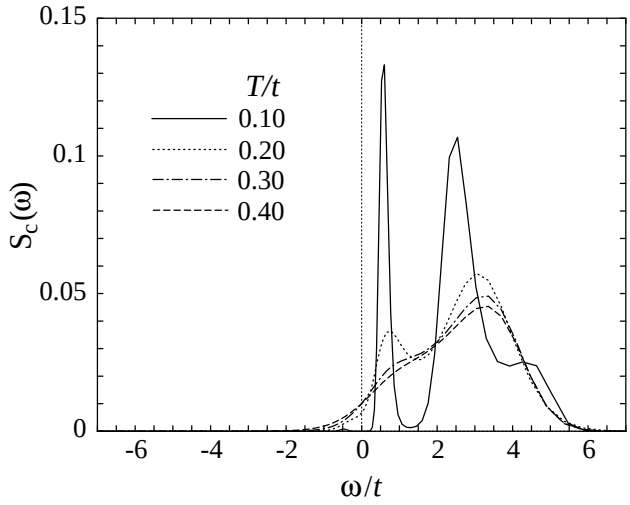

Figure 22. The dynamic spin structure factor of the conduction electrons, $S_c(\omega)$, in the half-filled one-dimensional Kondo lattice model; $J/t = 1.6$.

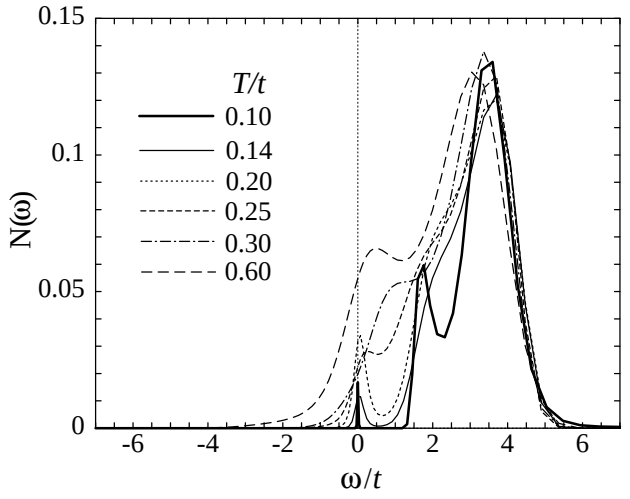

Figure 23. The dynamic charge structure factor of the conduction electrons, $N_c(\omega)$, in the half-filled one-dimensional Kondo lattice model; $J/t = 1.6$.

two clear peaks appear, a smaller peak at $\omega \sim 0$ and a bigger one at Δ_c. These two peaks originate from the sharp peak structure in $\rho(\omega)$ at $\omega = \pm\Delta_{qp}$. The excitations of thermally populated quasiparticles within the sharp peak in $\rho(\omega)$ contribute to the peak at $\omega = 0$, while the excitations between the peaks in $\rho(\omega)$ give rise to the peak in $N(\omega)$ at $\omega \sim \Delta_c$. With increasing temperature, the increased number of thermally populated quasiparticles enhance the peak at $\omega = 0$, but at the temperature $T \sim \Delta_s$ the peak structure is completely smeared out, which reflects the disappearance of the peak in $\rho(\omega)$. The gap structure of $N(\omega)$ and the energy scale of Δ_c become unclear at temperatures much smaller than Δ_c.

The dynamic quantities studied by the finite-T DMRG method have revealed the many-

body nature of the gap formation in the Kondo insulators. The difference among the excitation gaps depending on the channels is a characteristic feature of the Kondo insulators as compared with the ordinary band insulators. The temperature-induced gap formation for the single-particle density of states is further clear evidence of the many-body feature. Even at a fixed temperature a renormalized band picture fails to capture the essential physics of the strongly correlated insulators. A typical example is that the two-body excitation spectrum $N(\omega)$ is very different from a convolution of the one-body excitation spectrum $\rho(\omega)$. For the Kondo insulators there are several small energy scales, corresponding to the spin gap, the quasiparticle gap and the charge gap. Among them the lowest one, the spin gap, plays a special role. At temperatures higher than the spin gap, the excitation spectra in the charge sector are also modified strongly. This means that the whole excitation spectrum is reconstructed above the temperature corresponding to the lowest energy scale.

5. Summary and discussions

In this review we have discussed the Tomonaga–Luttinger liquid properties of the one-dimensional Kondo lattice model away from half-filling. In particular, it is concluded that there is a large Fermi surface in the ground state from an investigation of the spin and charge Friedel oscillations. At half-filling of the one-dimensional Kondo lattice model, the ground state is always an incompressible spin-liquid phase. Studies on the dynamic correlation functions have revealed the many-body nature of this insulating phase in several ways.

These developments have been achieved by applying the density matrix renormalization group method either to the Hamiltonian itself or to the quantum transfer matrix. In the problem of the Kondo lattice model, there appear small energy scales at low temperatures. This implies that the correlation lengths for various quantities are relatively long and therefore we need sufficiently large systems if we are to observe intrinsic properties. On the other hand, there are eight states per site in the Kondo lattice problem. Of course for a quantum spin-1/2 chain there are only two states per site. Exact-diagonalization studies can perform well for the latter, but only poorly for the former. In this situation the DMRG method shows its full advantage for the Kondo lattice model.

We would like to stress that now we can calculate dynamic quantities at finite temperatures by applying the finite-T DMRG method to the quantum transfer matrix. This method is free from statistical errors and the truncation errors are the only numerical errors. Therefore, a much better accuracy is obtained for the imaginary-time data, from which the corresponding spectral function may be obtained reliably through the maximum-entropy method. Another advantage of the finite-T DMRG method compared with the quantum Monte Carlo simulations is that we do not have the negative-sign problem for any quantum systems.

Generally speaking, more elaborate calculations are required for the finite-T DMRG method compared with the zero-temperature DMRG method. Finite-temperature properties, both static and dynamic, of the Tomonaga–Luttinger liquid phase are of great interest, and studies in this direction are now in progress. In the near future it will become possible to address these questions. The investigation of a completely fermionic model for heavy fermions, for example the periodic Anderson model, is also left for the future.

Acknowledgments

It is our great pleasure to acknowledge fruitful collaborations with Tetsuya Mutou, Tomotoshi Nishino, Manfred Sigrist, Matthias Troyer and Hirokazu Tsunetsugu. We also benefited from

discussions with Hiroshi Kontani and Beat Ammon. This work was financially supported by a Grant-in-Aid from the Ministry of Education, Science, Sports and Culture of Japan.

References

[1] Luttinger J M 1960 *Phys. Rev.* **119** 1153
[2] Yosida K 1966 *Phys. Rev.* **147** 223
[3] Ruderman M A and Kittel C 1954 *Phys. Rev.* **96** 99
Kasuya T 1956 *Prog. Theor. Phys.* **16** 45
Yosida K 1957 *Phys. Rev.* **106** 893
[4] Tsunetsugu H, Sigrist M and Ueda K 1997 *Rev. Mod. Phys.* **69** 809
[5] Tsunetsugu H, Hatsugai Y, Ueda K and Sigrist M 1992 *Phys. Rev.* B **46** 3175
[6] White S R 1992 *Phys. Rev. Lett.* **69** 2863
White S R 1993 *Phys. Rev.* B **48** 10 345
[7] Wang X and Xiang T 1997 *Phys. Rev.* B **56** 5061
[8] Shibata N 1997 *J. Phys. Soc. Japan* **66** 2221
[9] Shibata N, Ammon B, Troyer M, Sigrist M and Ueda K 1998 *J. Phys. Soc. Japan* **67** 1086
[10] Ostlund S and Rommer S 1995 *Phys. Rev. Lett.* **75** 3537
[11] Haldane F D M 1981 *J. Phys. C: Solid State Phys.* **14** 2585
[12] Ueda K, Nishino T and Tsunetsugu H 1994 *Phys. Rev.* B **50** 612
[13] Shibata N, Tsvelik A and Ueda K 1997 *Phys. Rev.* B **56** 330
[14] Schulz H J 1990 *Phys. Rev. Lett.* **64** 2831
[15] Shiba H and Fazekas P 1990 *Prog. Theor. Phys. Suppl.* **101** 403
[16] Moukouri S and Caron L G 1996 *Phys. Rev.* B **54** 12 212
[17] Shibata N, Ueda K, Nishino T and Ishii C 1996 *Phys. Rev.* B **54** 13 495
[18] Fabrizio M and Gogolin A O 1995 *Phys. Rev.* B **51** 17 827
[19] Egger R and Grabert H 1995 *Phys. Rev. Lett.* **75** 3505
[20] Egger R and Schoeller H 1996 *Czech. J. Phys. Suppl.* S4 **46** 1909
[21] Fujimoto S and Kawakami N 1994 *J. Phys. Soc. Japan* **63** 4322
[22] White S R and Affleck I 1996 *Phys. Rev.* B **54** 9862
[23] Sikkema A E, Affleck I and White S R 1997 *Phys. Rev. Lett.* **79** 929
[24] Yamanaka M, Oshikawa M and Affleck I 1997 *Phys. Rev. Lett.* **79** 1110
[25] Tsunetsugu H, Sigrist M and Ueda K 1993 *Phys. Rev.* B **47** 8345
[26] Caprara S and Rosengren A 1997 *Europhys. Lett.* **39** 55
[27] Honner G and Gulacs M 1998 *Phys. Rev.* B **58** 2662
[28] Kolomeisky E B and Straley J P 1996 *Rev. Mod. Phys.* **68** 175
[29] Bedürftig G, Brendel B, Frahm H and Noack R M 1998 *Phys. Rev.* B **58** 10 225
[30] Yu C C and White S R 1993 *Phys. Rev. Lett.* **71** 3866
[31] Tsvelik A M 1994 *Phys. Rev. Lett.* **72** 1048
[32] Fujimoto S and Kawakami N 1997 *J. Phys. Soc. Japan* **66** 2157
[33] Silver R N, Sivia D S and Gubernatis J E 1990 *Phys. Rev.* B **41** 2380
[34] Gubernatis J E, Jarrell M and Silver R N 1991 *Phys. Rev.* B **44** 6011
[35] Jarrell M and Gubernatis J E 1996 *Phys. Rep.* **269** 133
[36] Rice T M and Ueda K 1985 *Phys. Rev. Lett.* **55** 995
Rice T M and Ueda K 1986 *Phys. Rev.* B **34** 6420
[37] Igarashi J, Tonegawa T, Kaburagi M and Fulde P 1995 *Phys. Rev.* B **51** 5814
[38] Nishino T and Ueda K 1993 *Phys. Rev.* B **47** 12 451
[39] Lieb E H and Wu F Y 1968 *Phys. Rev. Lett.* **20** 1445
[40] Fye R M and Scalapino D J 1990 *Phys. Rev. Lett.* **65** 3177
Fye R M and Scalapino D J 1991 *Phys. Rev.* B **44** 7486
[41] Mutou T, Shibata N and Ueda K 1998 *Phys. Rev. Lett.* **81** 4939